Research Article

Andrey Alexandrovich Mongush, and Pascal Olschewski*

A new look at the geodynamic development of the Ediacaran–early Cambrian forearc basalts of the Tannuola-Khamsara Island Arc (Central Asia, Russia): Conclusions from geological, geochemical, and Nd-isotope data

https://doi.org/10.1515/geo-2022-0586
received June 02, 2023; accepted November 22, 2023

Abstract: Oceanic igneous rocks throughout the Altai-Sayan Fold Belt (ASFB) in central-southern Siberia are often considered to be late Precambrian–early Paleozoic accreted elements of oceanic crust – often of uncertain paleogeographic or geodynamic origin. We explore the role of suprasubduction zone settings in the formation of different ASFB terranes. Our study offers a non-accretionary perspective on the tectonomagmatic development of basalt-bearing units in the ASFB on the example of the forearc terrane of the Ediacaran–early Cambrian Tannuola-Khamsara island arc (herein termed Sayan-Tuvan forearc zone). We describe the geochemistry, structural geology, and stratigraphic relations of basalts of the Aldynbulak, Uttug-Khaia, and Chingin formations, which are integral parts of the Sayan-Tuvan forearc zone. The Aldynbulak basalt samples mainly fall in the compositional fields of ocean island basalts and enriched mid-ocean ridge basalts (E-MORB) and likely derived from a deep mantle source. The Uttug-Khaia and Chingin basalts are N- and E + T-MORB-like basalts, carrying forearc geochemical signatures. Specifically, the Chingin Formation contains boninite dikes and is associated with a boninite-bearing ophiolite. Boninites are commonly associated with forearc magmatism and thus a forearc formation setting is likely. Tectonic and stratigraphic considerations imply that the Aldynbulak basalts formed first, followed by the Uttug-Khaia and later the Chingin basalts and boninites. A schematic model, involving decompression melting of the mantle, is proposed for the development of the studied forearc basalt suites that are linked with the growth of the Tannuola-Khamsara island arc system 580–540 million years ago.

Keywords: Tuva, ophiolites, geochemistry, subduction initiation, forearc development

1 Introduction

Numerous studies indicate that the development of intra-oceanic subduction zones is accompanied by the formation of ophiolites [1–8]. Together with partial melting processes of the depleted mantle, deeply situated enriched mantle reservoirs may be involved in this process [9–13]. Basalts enriched with incompatible elements are commonly encountered in forearc terranes, including accretionary complexes of island arc systems in the Altai-Sayan Fold Belt (ASFB) and Central Asian Orogenic Belt in general. Their nature has been explained by the accretion of oceanic lava plateaus and island arcs during subduction and collision in previous publications [14–22]. In most reconstructions, a multitude of distinct island arcs, seamounts, ribbon continents, or oceanic crust fragments within the Paleo-Asian Ocean is shown, each with their own, but often, uncertain geological history and unclear paleogeographic relations, that collide during the latest Precambrian and early Paleozoic [23–26]. Accretionary and convergent tectonic mechanisms are undoubtfully important processes in the ASFB, and yet how these terranes evolved during those long-lived subduction-accretion processes and how ophiolite and paleo-spreading complexes formed have been less addressed for specific regions in detail. Considering

* **Corresponding author: Pascal Olschewski,** Department of Earth Sciences, Memorial University of Newfoundland, 9 Arctic Avenue, A1B 3X5 St. John's, NL, Canada; Eurasia Department and Beijing Branch Office, German Archaeological Institute, Im Dol 2-6, 14195 Berlin, Germany; Institute of Geological Sciences, Paleontology Section, Freie Universität Berlin, Malteserstrasse 74-100, 12249 Berlin, Germany,
e-mail: polschewski@mun.ca
Andrey Alexandrovich Mongush: Tuvinian Institute for Exploration of Natural Resources SB RAS, 117a International'naya Street, 667007 Kyzyl, Russia

that forearc ophiolites are thought to be more likely emplaced than mid-ocean ridge and back-arc ophiolites [6,27], ophiolitic rocks that developed during forearc spreading appear to be less well understood in the ASFB.

We distinguish "accretionary" models herein from "non-accretionary" models as scenarios in which terranes and subzones share a complex geodynamic evolutionary history, instead of being an amalgamation of unrelated lithosphere fragments within suture zone-like settings. However, "non-accretionary" settings also experienced a considerable tectonic deformation especially during early Paleozoic collisional events.

Two recent examples for "accretionary" models from this region are within the Dzhida island arc and Gorny Altai (Kuznetsk-Altai) systems (Figure 1a). For both terranes mantle plume magmatism, the formation of seamounts and the following incorporation into accretionary prisms play a central role [28,29]. In the Dzhida subzone, these primitive oceanic structures are suggested to have been superposed by later island arc volcanism [30]. The involvement of forearc magmatism has not been discussed to explain the co-occurrence of chemically different basalt suites, even though parts of the Dzhida and Gorny Altai zones are associated with forearc or subduction processes [28–30]. In contrast, a re-evaluation of existing data has stressed the likely importance of mantle plumes, subduction initiation, and suprasubduction zones throughout the Central Asian Orogenic Belt including the Dzhida subzone, Gorny Altai, and the area of this study [31,32]. The lack of new data and field observations from the vast area of the ASFB, however, complicate the detailed reconstruction of tectonomagmatic settings [24,32].

Our study attempts to provide an additional "non-accretionary" and co-evolutionary point of view of terranes in the ASFB, in which the emplacement of enriched basalts is associated not only with accretion but is also linked with subduction initiation and forearc spreading. These subduction processes led to the emplacement of island arc granites (Tannuola-Khamsara arc). The proposed forearc spreading processes are recorded in ophiolitic and basaltic rocks which are associated with the growth of the Tannuola-Khamsara island arc. The latest Precambrian and earliest Paleozoic Tannuola-Khamsara island arc and the associated accretionary, and forearc and back-arc zones, that are outlined in detail below, meet certain criteria that are suitable to explore our hypothesis. These include the occurrence of boninites, that are commonly formed during subduction initiation and forearc magmatism in oceanic settings [33,34], ophiolites and basalt suites that stand in a tectonostratigraphic relation to each other (Figure 1a, b, and d) [35,36], the age of the oceanic crustal fragments within the accretionary zone, which is similar to that of island arc granites of the Tannuola-Khamsara island arc [37–39], and the onset of widespread molasse sedimentation at least with the beginning of middle Cambrian [35,40] that forms a connection between these terranes.

Our findings create important implications for the paleogeodynamic and paleogeographic configuration of Ediacaran–early Cambrian tectonostratigraphic units of the ASFB. For a comprehensive understanding of the geology of this region and to facilitate further studies, relevant subzones and study sites are described in detail because descriptions of the outcrop localities and their geological histories are often published in Russian only.

2 Geological setting of the study area and sampling sites

Terranes of the larger Tuva-Mongolian island arc system of the Paleo-Asian Ocean form a major part of the Caledonides of the ASFB (Figure 1a). Fragments of this system were displaced relative to each other and spatially re-oriented during several tectonic episodes, making it difficult to draw conclusions on former paleogeographic connections [14]. The Tannuola-Khamsara island arc as part of the Tuva-Mongolian system, however, is relatively well preserved compared to other Ediacaran–Cambrian island arc systems in the ASFB [41]. Several geographical areas and terrane-like units have been identified (from northwest to southeast): The forearc system of the island arc, Tannuola-Khamsara island arc, and East Tuva back-arc zones (terranes), as well as the Tuva-Mongolia microcontinent (Figure 1b–d).

The forearc of the Tannuola-Khamsara island arc comprises a complex arrangement of various subunits (herein roughly summarized as Sayan-Tuvan forearc zone). The Sayan-Tuvan forearc zone extends in a north-easterly direction for about 500 km and includes the frontal Dzhebash accretionary complex/wedge, late Neoproterozoic, ophiolitic strata in the Kurtushiba subzone, the Chingin and Aldynbulak formations, younger early Cambrian igneous and sedimentary rocks and up to middle Cambrian volcano-sedimentary forearc-style basin deposits especially in the Khemchik-Tapsa and Systygkhem zones [14,42,43]. After the termination of subduction processes and onset of collisional mechanisms, the middle/late Cambrian to Silurian Khemchik-Systygkhem molasse basin developed [43], covering large portions of the forearc basin sediments and island arc rocks. The main phase of collision and orogenesis in this region took place during the middle to late Cambrian to early Ordovician [18,19] causing

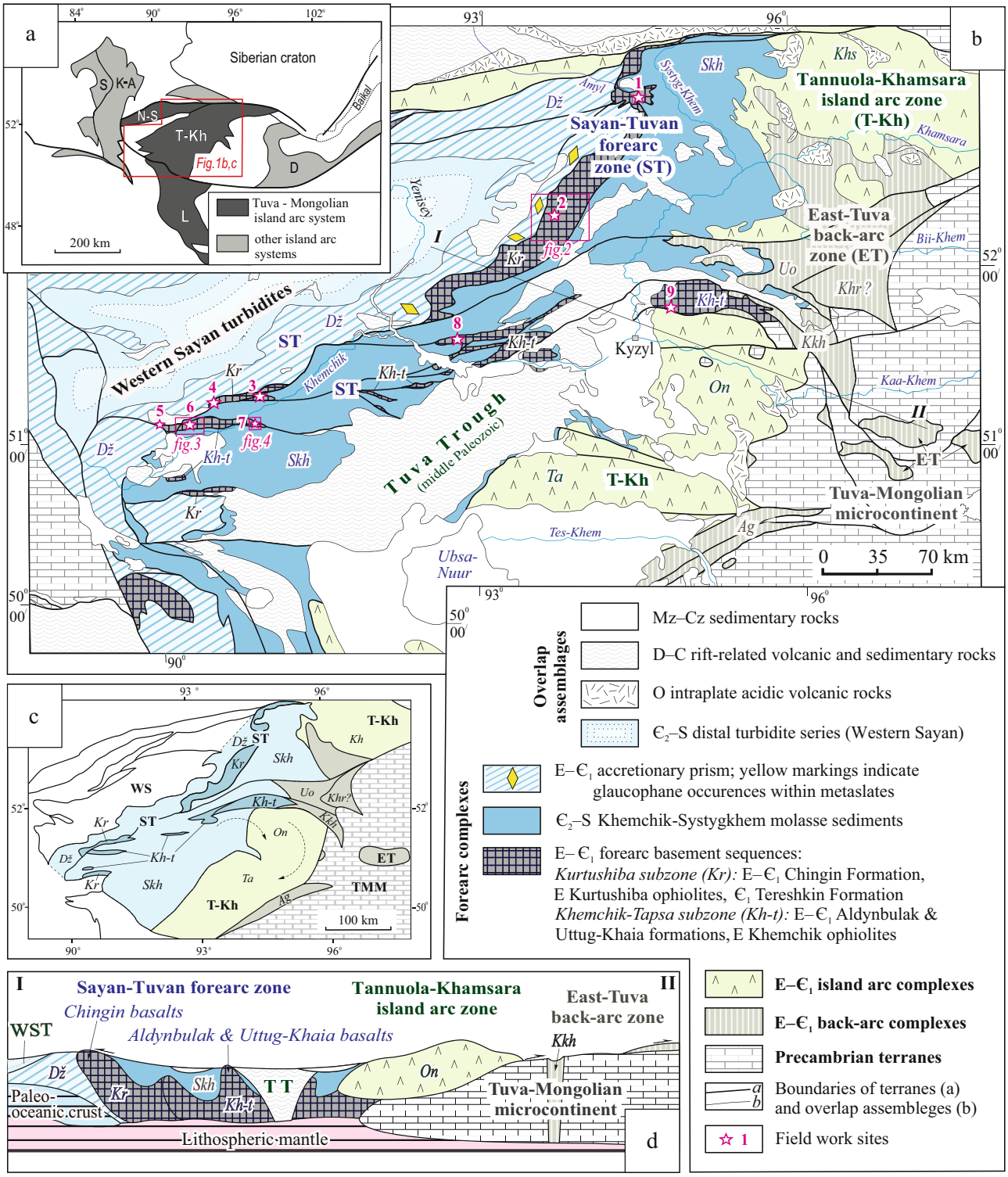

Figure 1: Geological and tectonic map of Western Sayan and Tuva. (a) Ediacaran–Cambrian island arc systems of the ASFB and Mongolia (compiled using data from [41]. Tuva-Mongolian island arc system terranes: T-Kh – Tannuola-Khamsara, N-S – North Sayan, and L – Lake Zone. Other island arc systems: S – Salair, Kuznetsk-Altai (K-A) and D – Dzhida (b) Geodynamic map of the Tannuola-Khamsara island arc terrane, including the accretionary prism, forearc and back-arc complexes (compiled using data from [43], Field work sites: 1 – Izinziul', 2 – Koiard, 3 – Saryg-Tash, 4 – Tlangara, 5 – Kopsek, 6 – Shat, 7 – Uttug-Khaia, 8 – Buura, 9 – Tapsa, note that the E-Є1 forearc basement sequences contain a complex system of tectonostratigraphic units which are not further differentiated on this map; (c) Terrane map of Tannuola-Khamsara island arc, including the adjacent East-Tuva back-arc zone. Abbreviations of the structural zones and respective subzones: S-T –Sayan-Tuvan forearc zone, *subzones*: Dž – Dzhebash, Kr – Kurtushiba, Kh-t – Khemchik-Tapsa, S-kh – Systygkhem; T-Kh – Tannuola-Khamsara island arc zone, *subzones*: Ta – Tannuola, On – Ondum, Khs – Khamsara; ET – East-Tuvan back-arc zone, *subzones*: Ag – Agardag, Kkh – Kaakhem, possibly Khr – Kharal, Uo – Ulugo; Precambrian terranes: TMM – Tuva-Mongolian microcontinent; WS – Western Sayan zone. Arrows indicate direction of block rotation during collisional episodes; (d) Schematic tectonic cross-section across the Sayan-Tuvan forearc, island arc, and back-arc system along the line I–II in (a). WST – Western Sayan turbidites. TT – Tuva Trough. E – Ediacaran, Є1 – lower Cambrian (approx. Terreneuvian – Cambrian Series 2), Є2 – middle Cambrian (approx. Cambrian Series 3), Є3 – upper Cambrian (approx. Furongian), O – Ordovician, S – Silurian, D – Devonian, C – Carboniferous, Mz – Mesozoic, Cz – Cenozoic (Figure 1a and c modified after [67], with kind permission from the Journal Geosphere Research).

widespread metamorphic overprints and tectonic distortion of all the abovementioned units.

The enriched basalts, focus of our study, comprise the Ediacaran–lower Cambrian Chingin Formation in the Kurtushiba subzone, as well as the Aldynbulak and Uttug-Khaia formations in the Khemchik-Tapsa subzone and partly the Dzhebash zone (Figure 1).

2.1 Frontal Dzhebash forearc subzone: Accretional basalts

This subzone is an accretionary zone, likely an accretion prism, which includes fragments of intraplate oceanic basalts (Figure 1b and d) [43]. It is composed of the Ediacaran–lower Cambrian Dzhebash (or Amyl) Group consisting of sharply variable slaty sedimentary rocks and basalts that were exposed to green- and blueschist metamorphic conditions. Glaucophane schists are localized along the contact to the Kurtushiba subzone (Figure 1b). The metasedimentary units consist of horizons of volcano-sedimentary rocks, cherts, marbles, marbled limestone, and thin lenses of ferruginous quartzites that are usually associated with metabasalts. The metabasalts are assumed to be part of an oceanic lava plateau which was accreted into the forearc zone during subduction. Analyses of the metabasalts have been published in previous studies [22,35,36,44], and thus, are not considered in detail herein.

2.2 The central forearc complex – the Kurtushiba subzone: Chingin basalts

This subzone is composed of tectonic slices and nappes of the Kurtushiba ophiolites and the volcano-sedimentary Chingin Formation, which were thrust to the west over the Dzhebash Group. A sharp angular discordance separates the Kurtushiba units and Chingin Formation from the overlying lower Cambrian volcano-sedimentary Tereshkin Formation (Figure 2). Enriched basalts of the Chingin Formation were sampled at the Izinziul', Koiard, Saryg-Tash, Tlangara, and Kopsek sites (Figures 1 and 2).

2.2.1 Izinziul' site

At the Izinziul' site, the Chingin Formation is a 4,400 m thick monoclinal fold dipping to the east at 45–60°. The formation is in tectonic contact with the Kurtushiba ophiolites in the west, and unconformably overlain by the middle-upper Cambrian terrigenous Alasug Group of the early Khemchik-Systygkhem molasse basin deposits [45] to the east. The Chingin Formation is partitioned into sub formations which are simply termed the "Lower Subformation" (3,400 m) that is conformably overlain by the "Upper Subformation" (1,000 m). Within the Chingin Formation system, the lower subformation is in general considerably thicker than the upper subformation. The lower subformation chiefly consists of basaltic lavas and tuffs, as well as interlayers of tuffaceous sandstones and undifferentiated siliceous rocks. Porphyritic pyroxene basalts of the lower subformation exhibit a concentration of SiO_2 = 50–54 wt%, a high concentration of MgO = 8–13 wt%, and a low concentration of TiO_2 = 0.3–0.5 wt%. These rocks are defined as boninites [45]. Igneous rocks of an enriched mid-ocean ridge basalts (E-MORB) like composition, however, predominate the basaltic units of the lower subformation while boninites only occur in a relatively smaller amount. The upper subformation of the Chingin contains carbonaceous, siliceous, tuffaceous clay shales, to a lesser extent basalt, tuffs, metagreywackes, and gravelites, as well as black dolomites [22,45]. Sampling of the lower subformation of the Chingin Formation was carried out along the northern part of the Izinziul' River Valley.

2.2.2 Koiard site

The Koiard site is a large, northwest dipping overturned fold, close to the metasedimentary units of the Dzhebash subzone (Figures 2 and 5). The Chingin Formation occurs in the limbs of the fold and the Kurtushiba ophiolites in the core area [46]. At this locality, the Chingin Formation is in conformable contact with strata of the Kurtushiba ophiolite. Porphyritic (KK-17/16) (Figure 5a) and aphyric (KK-18/16) pillow basalts of the upper subformation of the Chingin were sampled at Koiard. The pillow basalts are interbedded with tuffs. The pyroxenes in one basalt sample from the upper Chingin Formation at the Koiard site display a spinifex texture but the chemical composition does not correspond to that of komatiites [47]. However, komatiites have been reported from the Chingin Formation and other areas of the Kurtushiba subzone from exploration expeditions [47,48], but were not studied in detail and their origin is elusive. Possibly, the skeletal and spinifex-like textures are explained best with rapid cooling of the Chingin basalts.

2.2.3 Saryg-Tash, Tlangara, and Kopsek sites

In the southwestern part of the Kurtushiba subzone, small fragments of the Chingin Formation and Kurtushiba

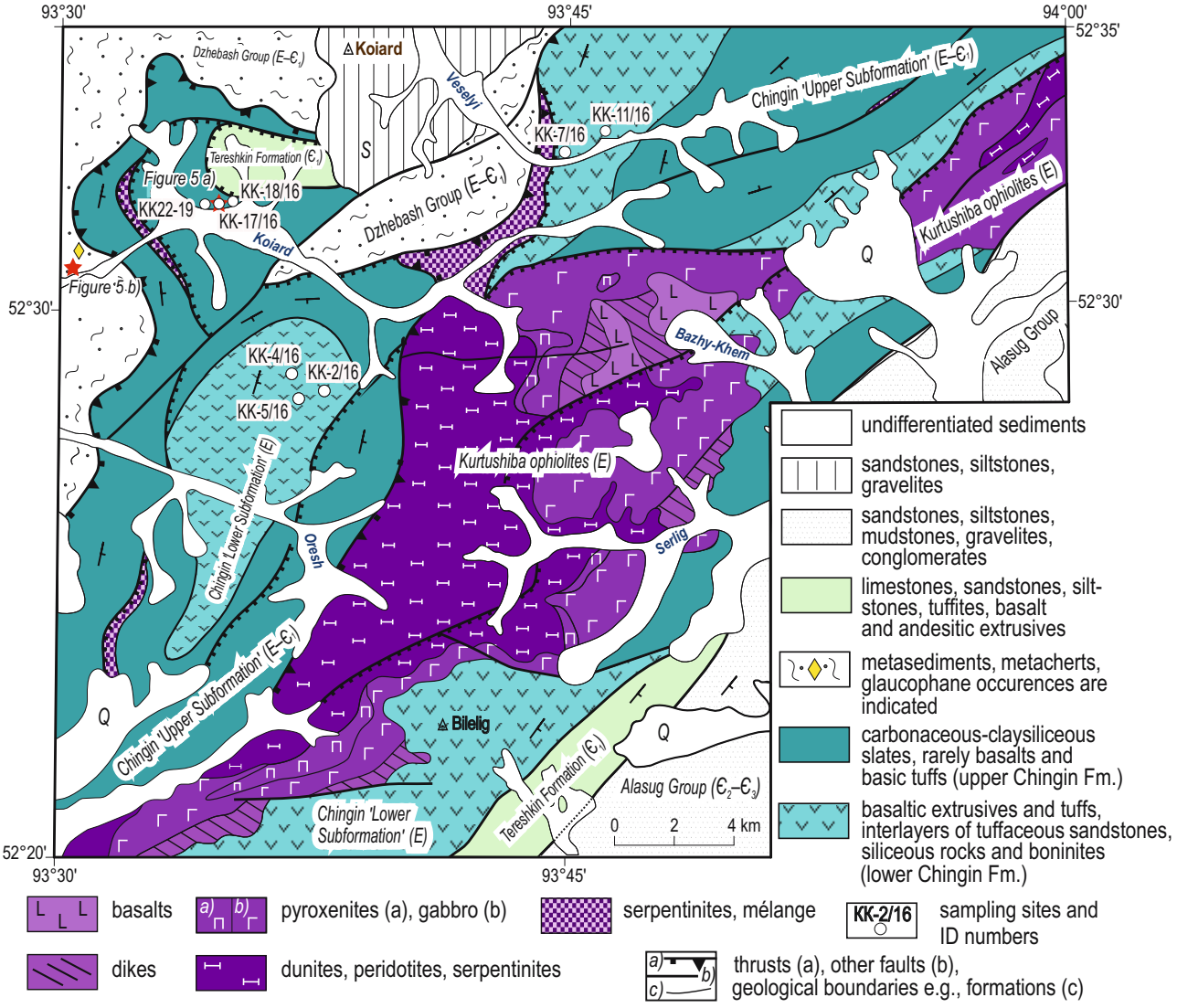

Figure 2: Geological map of the Koiard site (compiled using data from [22] and unpublished data by Yakov Sarbaa from prospecting expeditions at a scale of 1:50,000, 1973). Photographs of field sites are indicated. E – Ediacaran, $Є_1$ – lower Cambrian (approx. Terreneuvian – Cambrian Series 2), $Є_2$ – middle Cambrian (approx. Cambrian Series 3), $Є_3$ – upper Cambrian (approx. Furongian), S – Silurian (Khemchik-Systygkhem molasse basin sediments), Q – Quaternary.

ophiolites are present, which are exposed as discontinuous bands along the contact zone to the Dzhebash Group and early Paleozoic Khemchik-Systygkhem molasse basin deposits (Figure 1). In this area, the Chingin Formation crops out at the Saryg-Tash, Tlangara, and Kopsek sites (Figure 1b). Saryg-Tash is a complex anticlinal structure. The limbs of the anticline are folded middle Cambrian–Silurian sediments. In the axial part, podiform blocks with a width of 0.1–0.5 km protrude the Ordovician bedrock (conglomerates and sandstones) and consist of foliated Chingin basalts, massive serpentinites, pyroxenites, gabbroids, diorites, listwänites, and listwänitized rocks. At Tlangara, a serpentinite mélange with a thickness of ~100 m contains blocks of Chingin basalts, 40 × 60 m in size. At Kopsek, Chingin basalts are present as inclusions in a serpentinite mélange that is framing an ophiolite allochthon, as well as in the form of olistoliths among the Dzhebash metasediments.

2.3 Rear part of the Sayan-Tuvan forearc zone – the Khemchik-Tapsa zone: Aldynbulak and Uttug-Khaia basalts

The Khemchik-Tapsa subzone consists of several narrow, subparallel aligned outcrops of magmatic and sedimentary

units that underly the Khemchik-Systyghem molasse basin (Figure 1b and c). This subzone forms large anticlinal structures that comprise the late Ediacaran Khemchik ophiolites, the Ediacaran–lower Cambrian Aldynbulak and Uttug-Khaia sedimentary and basalt-bearing formations with a wide range of lithologies that include olistostromes, volcanic and volcanosedimentary rocks, early Cambrian gabbroids, and serpentinite mélanges. The Khemchik system is located between the central forearc complex (the Kurtushiba subzone) and the Tannuola-Khamsara island arc, while the Tapsa system is located closer to the island arc (Ondum subzone, Figure 1c). Associated with the Khemchik-Tapsa subzone is the conglomeratic early Cambrian Bayankol Formation that was laid down proximal to the Tannuola-Khamsara island arc and encompasses boulders of Neoproterozoic–early Cambrian igneous and sedimentary rocks derived from the Ondum subzone of the arc (Figure 1b) [14,42,49,50].

Enriched basalts are mainly found in the Aldynbulak Formation, which was studied at the Shat, Buura, and Tapsa sites (Figures 1 and 3). Similar to the Chingin Formation, the Aldynbulak Formation is subdivided in two formations. In general, the Aldynbulak Formation is comparable to the binomial structure and lithology of the Chingin Formation. There is, however, no reliable data available of the upper Aldynbulak basalts and boninites are also not known from this formation. The rocks of the Aldynbulak Formation experienced a considerable syn- and postdepositional tectonic history. Together with the Khemchik ophiolites, fragments of the Aldynbulak Formation are often encountered in Ediacaran–earliest Cambrian olistoliths. Complete sections have been preserved in particular at the Shat site and approx. 15 km to the east of it (Figure 3).

2.3.1 Shat study area

The thickness of the Aldynbulak Formation at the Shat site (Figures 3 and 5c) is about 3,000 m. It consists mainly of the basaltic “Lower Subformation” and a largely sedimentary “Upper Subformation.” The subformations are equally thick at the study locality. The lower subformation of the Aldynbulak Formation is dominated by pillow lavas, which are

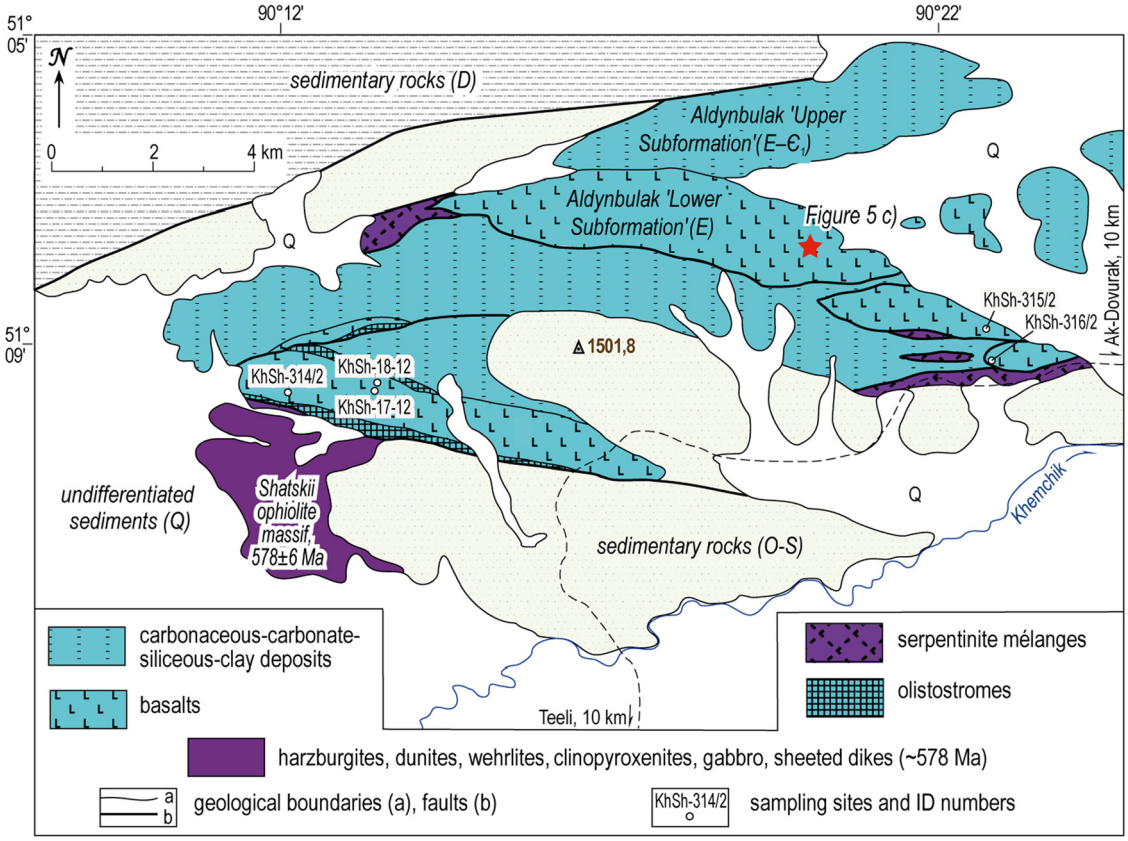

Figure 3: Geological map of the Shat site. Photographs of field sites are indicated. E – Ediacaran, $Є_1$ – lower Cambrian (approx. Terreneuvian – Cambrian Series 2), O – Ordovician, S – Silurian (O – S Khemchik-Systygkhem molasse sediments), D – Devonian (Tuva trough, rift-related deposits), Q – Quaternary.

associated with tuffs, tuffaceous sandstones, tuff breccias, as well as undifferentiated siliceous and carbonate rocks. The upper subformation consists of slaty siliceous rocks and metapelites with rare interlayers of carbonaceous black metashales, as well as single, smaller (~1 m thick) limestone horizons.

At Shat, the tectonic contact of the Aldynbulak Formation with the Khemchik ophiolites (Shatskii massif) is marked by narrow bands of olistostromes and serpentinite mélanges (Figure 3). The foliated sand-silt matrix of the olistostromes contains meter- to tens of meter-sized blocks of cherts and basalts, as well as altered ultrabasites, gabbroids, and limestones [51]. The serpentinite mélange zone is tens to hundreds of meters thick, with inclusions of basalts, quartzites, massive serpentinites, and limestones. The sampling points are shown in Figure 3.

2.3.2 Buura site

At the Buura study area, lower Cambrian strata comprise reworked fragments of the Aldynbulak Formation in an olistholithic setting. The sedimentary units are siltstones, sandstones, gravelites, and conglomerates as well as blocks of limestone, chert, basalt, sometimes gabbro, and ultramafic rocks. The sampling of Aldynbulak basalts was carried out on the largest olistolith block with pillow basalts, measuring about 500 m across.

2.3.3 Uttug-Khaia formation and Uttug-Khaia mountain

In previous mapping projects considering the southeastern edge of the Western Sayan mountains (Figure 1), most Ediacaran–lowermost Cambrian sedimentary and basalt-bearing units have either been attributed to the Aldynbulak or Chingin Formations or synonymous formations of these [14,35–37,42,49]. Geochemical analytics of different localities of the Aldynbulak Formation basalts (this study) have, however, shown that these basalts do group into two different geochemical variants. We thus preliminarily subdivided the Aldynbulak Formation into the Aldynbulak and Uttug-Khaia Formation (with lower and upper subformations), based on the different chemical basalt compositions and the implication that these formed in different geodynamic environments.

The Uttug-Khaia Formation basalts (Figure 5d) are best exposed at the Uttug-Khaia Mountain locality within the Khemchik-Tapsa zone (Figure 4). At Uttug-Khaia Mountain, fault-bound tectonic sections of basalt-bearing volcano-sedimentary and sedimentary rocks are found alongside the olistolithes. The basalt-bearing volcano-sedimentary units are composed of pillow lavas, foliated basaltic tuffs, interlayers of cherts, and layers of siliceous volcanogenic rocks and siliceous carbonates. The pillow lavas are cut by single dikes of plagiophyric basalts. Other sedimentary rocks are largely undifferentiated cherts. The matrix of the olistostromes is a sedimentary breccia and conglobreccia with fragments of basalts, less often cherts, carbonate rocks, and (meta-)shale (Figure 5e and f). Clastic blocks indicating episodes of considerable mass-transport are up to several tens of meters in size, composed mainly of cherts, as well as limestones, dolomites, and less often gabbroids and serpentinite. Some siliceous olistoliths are monolithic breccias composed of flints in a siliceous cement (Figure 5f). The Ediacaran–lower Cambrian Uttug-Khaia Formation is overlain by siliciclastic and reef carbonates of the Akdurug Formation from which archaeocyathids of the Sanashtykgol biohorizon (Siberian stage Botoman) have been described [40]. The lower units of the Akdurug Formation show signs of reworking of the underlying olistoliths [42]. The sampling localities are shown in Figure 4.

2.3.4 Tapsa River site

The study locality in the Tapsa River area is located further east than the previously described sites. Here lower Cambrian olistostromes are in direct contact with the island arc complexes of the Ondum subzone (Figure 1b, locality 9). The volcano-sedimentary units are mainly conglomerates, gravelites, sandstones, and siltstones. The mass-transport related deposits include blocks of 1–30 m in size, composed of island arc basalts and plagiorhyolites, limestones, as well as Aldynbulak basalts (sample Tp-3/2).

2.3.5 Rear part of the Sayan-Tuvan forearc zone – the Systygkhem subzone

The crustal rocks of the Sayan-Tuvan forearc are largely covered by the Khemchik-Systygkhem molasse basin deposits in the Systygkhem subzone and not further considered in this study (Figure 1b–d).

The Chingin, Aldynbulak, and Uttug-Khaia Formations, together with the Tannuola-Khamsara island arc and back-arc complexes are overlain by sedimentary and volcano-sedimentary deposits of late Early Cambrian age (roughly Cambrian Age 2–4, ca. 521–509 Ma; [52] mainly the – Tereshkin, Bayankol, Akdurug, Ilchir, Syynak, Irbitei, Terektig, and similar formations [35,36,40,42]. It has been inferred from stratigraphic reports [35,36] (and references therein), tectonic configurations, and provenance studies [50] that these

sediments were formed by extremely proximal sources and accumulated in an active margin forearc-like basin setting [43,53]. Sedimentary, tectonic, and volcanic processes were presumably controlled by unstable subduction, possibly due to subduction slowdown and slab separation (slab window formation) [54].

2.4 Understanding the architecture of the Ediacaran ophiolites in Tuva and western Sayan

Approximately 80 major mafic-ultramafic massifs have been reported from Tuva and the bordering Western Sayan region [55]. Only very few of these massifs were studied extensively, their age and geological history often being speculative. Thus, a comprehensive insight into the various ophiolitic sequences is vital to understand the development of this region and the meaning of the herein studied basalts. Here we provide a brief review and overview of relevant ophiolitic complexes in the larger Sayan-Tuvan forearc zone and associated terranes.

2.4.1 Ophiolites in the Kurtushiba area

The Kurtushiba ophiolites (Figures 1 and 2) (associated with the Chingin basalts) were likely formed during subduction

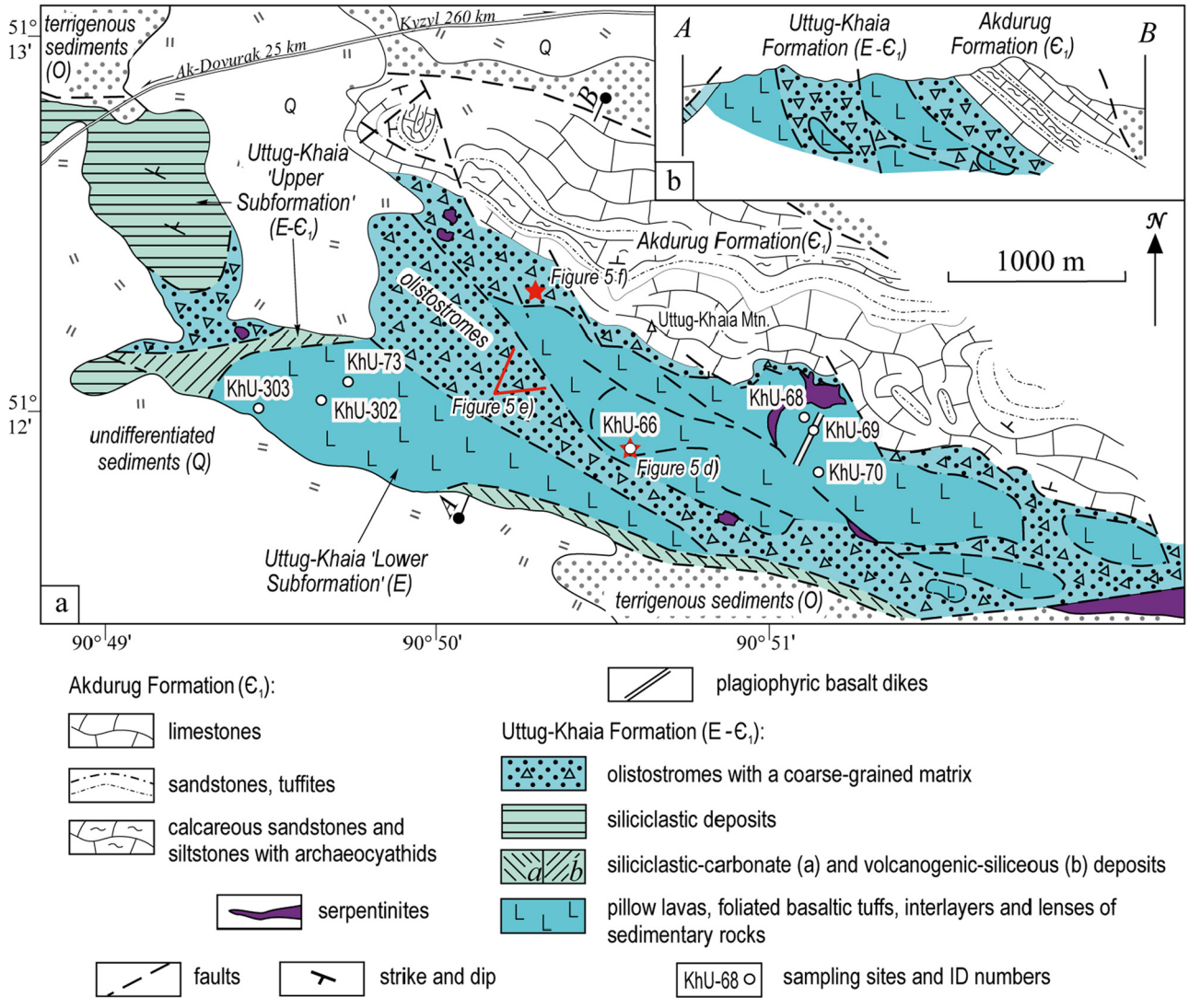

Figure 4: Geological map and section of Uttug-Khaia site (compiled and adapted from [42] with kind permission from the Journal Geologiya i Geofizika). Photographs of field sites are indicated. (a) Geological map showing outcrops of the Uttug-Khaia Formation (formerly assigned to the Aldynbulak Formation) and sampling localities; (b) Section A–B through the Uttug-Khaia Mountain fold system displaying the stratigraphic relations of the different complex faulted units. E – Ediacaran, $Є_1$ – lower Cambrian (approx. Terreneuvian – Cambrian Series 2), O – Ordovician (Khemchik-Systygkhem molasse sediments), Q – Quaternary.

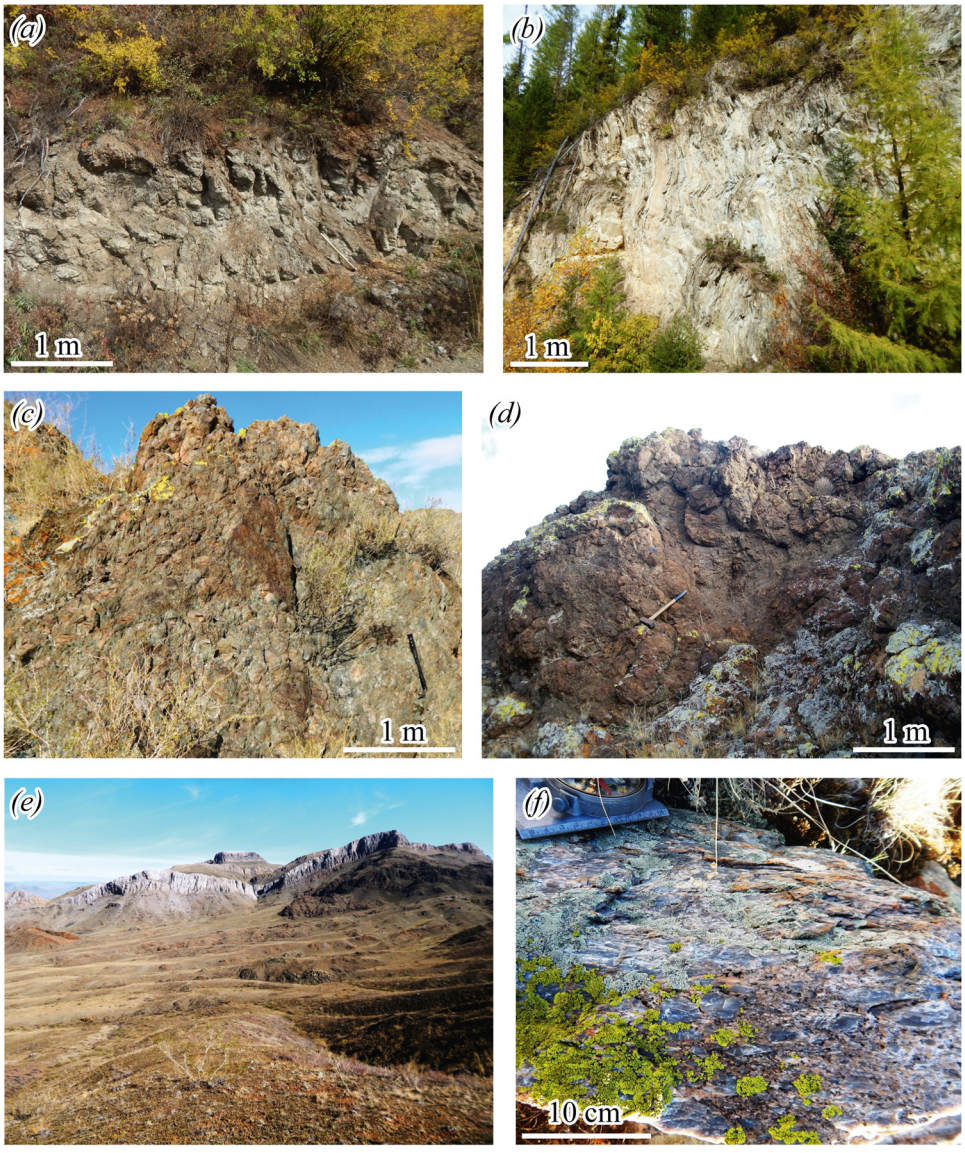

Figure 5: Field photographs of the study sites. (a) Chingin pillow basalts at Koiard; (b) Dzhebash metasediments (slate) at the Koiard site; (c) Aldynbulak pillow basalts at Shat; (d) Uttug-Khaia pillow basalts at the southern foot of Uttug-Khaia Mountain; (e) Uttug-Khaia section: olistostromes in the foreground and the overlying lower Cambrian conglomeratic and archaeocyathid bearing Akdurug Formation in the background; (f) Olistolith breccia with siliceous clasts in a siliceous matrix, Uttug-Khaia section. ((a) and (b) in Figure 2; (c) in Figure 3; (d)–(f) in Figure 4).

initiation and the onset of primitive ensimatic island arc formation. They contain younger boninites and older MOR-type basalts [56,57]. The co-occurrence of sheeted dike complexes that exhibit oceanic as well as island arc geochemical signatures [22,57] implies different formation settings of the ophiolitic basalts. Indirect evidence for a multi-generation development of the Kurtushiba ophiolites is given by magmatic breccias that comprise fragments of serpentinites in clinopyroxenites, fragments of pyroxenites and gabbro in plagiogranites, and gabbro and diabase set in a diabasic matrix [57], as well as ultramafic xenoliths in gabbro. In some cases, dunites were intruded by gabbroid and troctolitic rocks which led to the alteration of these dunites to rocks with wehrlitic and clinopyroxenitic composition [44,58].

2.4.2 Khemchik area ophiolites

The formation of the Khemchik ophiolites (Figures 1, 3 and 4) (linked with the Aldynbulak and Uttug-Khaia basalts) also took place during the development of the primitive island arc [37], but there is evidence for an inter-arc or back-arc origin [31,57]. The Khemchik ophiolites differ from the ones occurring in the Kurtushiba zone (Figure 1)

by an increased amount of andesite, microdiorite, quartz microdiorite, and plagiogranite dikes [37]. In contrast, only single plagiogranite veins were found in the Kurtushiba ophiolites. The Khemchik ophiolites are characterized by a more pronounced Nb-Ta negative anomaly in comparison to the Kurtushiba ophiolite units [59]. Ar–Ar dating of amphibole from the Shatskii massif gabbro (Figure 3) revealed an age of 578.1 ± 5.6 Ma for the Khemchik ophiolites [37]. It is noteworthy that the sheeted dike complex in the Shatskii massif is not uniform, similar to those of the Kurtushiba ophiolite. The dikes exhibit different orientations and petrologic characteristics, indicating that this ophiolite evolved substantially during different episodes of growth [57].

The distribution of trace elements in the gabbro and dike complexes of the Khemchik ophiolite is similar to that of N-MORB, but the concentration of elements is lower than in N-MORBs, and they show a slight negative Nb anomaly [37,59]. A negative Nb–Ta (or Nb) anomaly is probably one of the most important geochemical signatures of magmas produced in subduction zones [60,61] and is seen, for example, in the forearc magmatic rocks of the Bonin-Mariana arc [62].

2.4.3 Origin of the Kurtushiba and Khemchik ophiolites

So far, it is unclear how the Kurtushiba and Khemchik ophiolites relate to the Tannuola-Khamsara island arc system. Berzin and Kungurtsev [14] and Berzin [43] understand the Kurtushiba and Khemchik ophiolites as part of the accretional prism area that possibly represent "accretion type" ophiolites (sensu [11]). This approach implies that these ophiolites in the Sayan-Tuvan forearc zone may not necessarily origin from the subduction processes adjacent to the Tannuola-Khamsara island arc, but instead represent random oceanic crustal parts of the Paleo-Asian Ocean stacked up during later tectonics. However, there are various indicators which suggest that the Kurtushiba and Khemchik ophiolites are not allochthonous fragments and more likely formed in association with the Tannuola-Khamsara island arc and subduction systems. The geochemical composition of plagiogranites, andesites, and diabases of these ophiolites are very similar or identical with equal rocks found in the Ondum subzone of the Tannuola-Khamsara island arc. The age range of the oldest granites in the Ondum subzone (572–562 Ma) is comparable with that of the Shatskii massif (578 Ma) and the late-early to middle Cambrian stratigraphic overlap assemblages throughout this region contain recycled material of the underlying (ophiolitic) strata [35–39,59] These connections and similarities were best explained, given the tectonostratigraphic arrangement of the ASFB terranes in that area, if the Kurtushiba and Khemchik ophiolites were created in the incipient and expanding proto-arc–forearc region of the Tannuola-Khamsara island arc. Samples of both ophiolite complexes are of forearc plateau basalt affinity [59].

2.4.4 Ophiolites in the back-arc subzone of the Tannuola-Khamsara island arc

The back-arc–forearc subtype of suprasubduction ophiolites (for definition of this type see [31]) is located in the Agardag back-arc subzone (Figure 1b). The age of the Agardag ophiolites has been constrained by dating a plagiogranite dike associated with the gabbro of the ophiolite massif (569.6 ± 1.7 Ma, Pb–Pb dating of zircons) and Sm-Nd age for the gabbro of the Karashat ophiolite massif (546 ± 18 Ma) [63]. The straight nature of the dated plagiogranite dike may also indicate that the host ophiolite is older than 570 Ma [63]. Detrital zircon age spectra from the Terektig Formation of the Agardag subzone do suggest that the Agardag ophiolite is slightly older than 570 Ma [63] (580–574 Ma [64]), which is similar to the age of the Khemchik ophiolites (Shatskii massif, 2.4.2). It has been proposed that basalt dikes and lavas exposed on the northern side of the Teskhem River (Figure 1b) are part of ophiolites [63,65,66]. On the other hand, the lower Cambrian volcanic Karakhol and the archaeocyathid-bearing Terektig formations were mapped (Gibsher et al. 1987 unpublished, map published in [67]) at exactly the position used for the subsequent studies [63,65,66]. The age of the Karakhol and Terektig formations is approximately ~525–509 Ma [67] or ~530–520 Ma [64] and according to available geochemical datasets, the volcanic rocks of the Karakhol Formation were formed in an active continental margin setting [67]. Yang et al. [32], however, interpret the Agardag zone as suprasubduction-related terrane. The likely broader involvement of subduction-processes has also been acknowledged by Pfänder and Kröner [63]. According to Dobretsov et al. [16], the Agardag ophiolites formed during rifting of continental lithosphere are comparable to the rifting system of the modern Red Sea. This shows the need for a reevaluation of the Agardag mélange-suture zone and creation of a detailed geological framework in order to understand its complex geological history and relation to adjacent terranes.

The Ediacaran–lower Cambrian Kuskunnug Formation is also part of the Agardag back-arc subzone. There, ocean

island basalts (OIB) and E-MORB-like rocks have been identified in the eastern part of the Teskhem River site, as well in blocks within the mélanges of the Agardag site [16,64,66,67]. Considering the age, geographical distribution of these geodynamic units, and their relative location to the Dzhebash accretional zone and Tannuola-Khamsara island arc, it implies that the Ediacaran–early Cambrian Chingin, Aldynbulak (and Uttug-Khaia), and Kuskunnug volcanogenic formations (which all contain enriched basalts) may have formed in a related process, but at different distances in relation to the subduction zone.

Ophiolites of the Kaakhem back-arc subzone (Figure 1b–d) have been found to carry similar geochemical signatures like the enriched back-arc basalts of the Woodlark Basin in the southwestern Pacific Ocean, that was formed during spreading processes involving the subcontinental lithosphere (in the case of the Kaakhem subzone, the Tuva-Mongolian microcontinent) [16]. The lower Cambrian carbonate-terrigenous Tapsa Formation is associated with the Kaakhem subzone [68], which suggests that the age of the Kaakhem ophiolites is comparable to that of the Tapsa Formation.

3 Methods

3.1 Analytical techniques

Thin section analyses were performed according to the standard procedures.

Major elements were determined by X-ray fluorescence at the Institute of Geochemistry, Irkutsk and the Institute of Geology and Mineralogy, Novosibirsk, Russia. Trace elements were measured by standard inductively coupled plasma mass spectrometry techniques using an Agilent 7500c MSr at the Limnological Institute in Irkutsk, on a Finnigan Element setup at the Analytical Center of the Institute of Geology and Mineralogy in Novosibirsk, and on a PlasmaQuard 3 “VG Elemental” MS at the Institute for Analytical Instrumentation, St. Petersburg. The acquired measurements for the same samples at three different laboratories yielded satisfactory and consistent results.

The Sm-Nd data were obtained at the Geological Institute (Kola Science Center) in Apatity, Russia. The Sm and Nd isotope compositions were measured on a Finnigan-MAT 262 (RPQ) MS in a static regime. The blank sample contained 0.03–0.2 ng Sm and 0.1–0.5 ng Nd. The accuracy of determination was as followed: Sm and Nd concentrations ± 0.5%, 147 Sm/144 Nd ± 0.5%, and $^{143}Nd/^{144}Nd$ ± 0.005% (2σ).

4 Results

4.1 Petrography of basalts

The *Chingin basalts* are massive or foliated and often small-amygdaloidal (0.3–2.5 mm). In general, these basalts experienced greenschist metamorphism although primary microstructures are still recognizable (Figure 6a–c). Porphyritic textures are common, with phenocrysts of plagioclase (Figure 6d) and clinopyroxene (0.5–2.5 mm). Localized Chingin basalts were affected by a metamorphic greenschist facies overprint and transformed to albite-chlorite-epidote-actinolite rocks with a slaty appearance. However, pillow basalts were still identifiable in the field.

The *Aldynbulak basalts* (Figure 6e and f) are aphyric to porphyritic pillow lavas. Even though less affected by low-temperature metamorphosis in comparison to the Chingin basalts, secondary minerals can be a significant component of the Aldynbulak basalts (up to 50% in thin section). Intersertal microstructures are characteristic of the groundmass. In porphyritic variants, plagioclase crystals are 0.5–6.0 mm large. Also, microporphyritic chlorite mineral aggregates (0.5 mm) show an olivine habitus (at the Buura site, olivine is present in the normative composition of the rock).

The *Uttug-Khaia basalts* are massive and small-amygdaloidal, aphyric, ophitic (Figure 6g) and small-porphyritic pillow lavas with unaltered clinopyroxene and albitized plagioclase. In porphyritic basalt samples, plagioclase and clinopyroxene are 1–2 mm large. About 5% of the rock samples are amygdales with an average size of 0.3–0.8 mm in diameter. They are filled with chlorite and calcite or palagonite. Palagonite is also found in the intergranular spaces of plagioclase crystals in an amount of up to 1% (Figure 6h).

The *Uttug-Khaia basalt dikes* (Figure 6i) are massive porphyritic rocks with albitized plagioclase (1–1.5 or 4–7 mm large). The groundmass has a poikilophitic texture and consists of plagioclase laths and clinopyroxene oikocrysts, as well as a small amount of volcanic glass replaced by fine-flakey chlorite. Under the petrographic microscope, the Uttug-Khaia dikes are comparable with the less altered and metamorphosed versions of the studied forearc basalts.

The major and trace element composition does not differ fundamentally between metamorphic and non-metamorphic rocks of the Aldynbulak and Chingin formations (Table 1). Very likely, the Sayan-Tuvan forearc zone basalts were subject to localized tectonic systems which caused the metamorphism and hydrothermal alteration of some outcrops, while others remained largely unaffected.

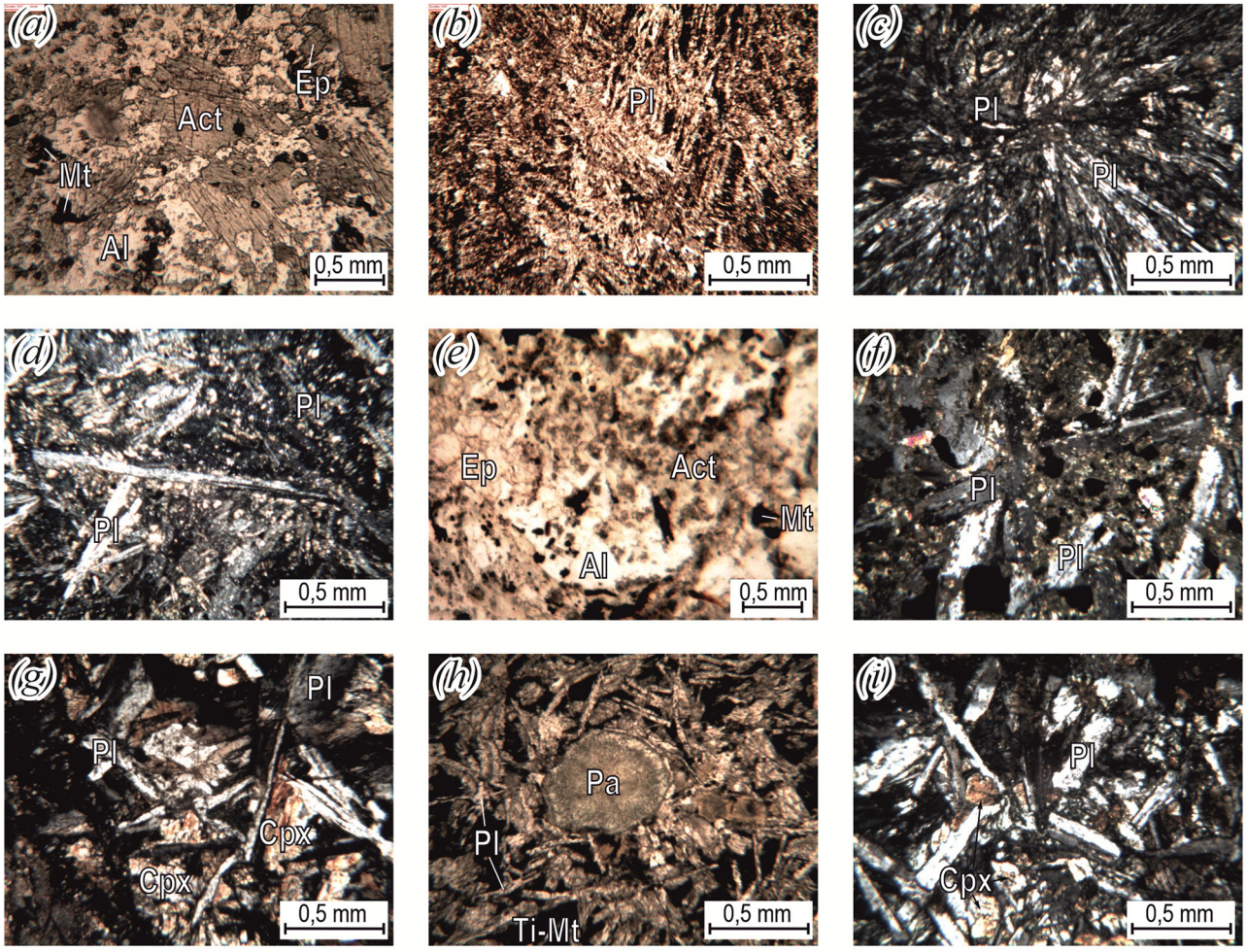

Figure 6: Micrographs of the Chingin (a)–(d), Aldynbulak (e) and (f), and Uttug-Khaia basalts (g)–(i). (a), (b), (e), and (h) were taken plain polarized light, while all others were taken with crossed Nicols. (a) KI-331/1 - albite-epidote-actinolite metabasalt; (b) KK-2-16 - actinolitized and epidotized basalt with relics of varioles; (c) KKp-2-12 - spherulitic and variolitic basalt fabrics; (d) KK-17-16 - needle shaped plagioclase phenocrysts; (e) KhSh-314-2 - actinolite-chlorite-epidote metabasalt; (f) Kh12-316-2 - albitized plagioclase in a porphyritic sample; (g) KhU-66/12 - ophitic basalt; (h) KhU-303 - basalt with palagonite; (i) KhU-69/12 - porphyry basalt (dike). Abbreviations: Al – albite, Act – actinolite, Cpx – clinopyroxene, Ep – epidote, Pl – plagioclase, Pa – palagonite, Mt – magnetite, and Ti-Mt – titanomagnetite.

4.2 Geochemistry

4.2.1 Major and trace element contents of the basalts

Aldynbulak basalts. The Aldynbulak basalts are alkaline to subalkaline rocks and plotted in the fields of trachybasalt and basalt on a $Na_2O + K_2O$ vs SiO_2 diagram (Figure 7a and b) (after [69]). A large diversity and spread of major elements (low to high aluminum Al_2O_3 = 11.6–21.5 wt%, moderate to ultra-titanium TiO_2 = 1.6–4.5 wt%, low to ultra-potassium K_2O = 0.20–2.63 wt%) mainly reflects the varying geochemical compositions of the different Aldynbulak sampling sites. On a Nb/Th vs Zr/Nb diagram (after [70]), the Aldynbulak basalts occupy a boundary position between the fields of the oceanic island basalts and oceanic plateau basalts (Figure 9a) and in a ternary graph Nb*2–Zr/4–Y (after [71]), the Aldynbulak samples are plotted in the fields of intraplate alkaline basalts and intraplate tholeiites (Figure 9b). The elemental ratios La_n/Yb_n = 3.0–12.8 and Th_n/Yb_n = 2.6–9.4 (Table 1) suggest an OIB and E-MORB-like geochemical composition (OIB: La_n/Yb_n = 11.7 and Th_n/Yb_n = 10.1 [72]; E-MORB: La_n/Yb_n = 2.9 and Th_n/Yb_n = 2.2 [73]). These results are supported by a Tb*3–Th–Ta*2 ternary diagram (Figure 9c) (after [74]) and the spider diagrams (Figure 8a and b) in which the Aldynbulak samples mainly overlap with OIB and E-MORB-like basalts.

Uttug-Khaia basalts. The basalts and basaltic andesites (Figure 7) of the Uttug-Khaia Formation are marked by low Al_2O_3 = 13.1–15.2 values. TiO_2 = 1.44–2.44 and K_2O = 0.13–1.13 wt% is on average lower compared to the Aldynbulak

Table 1: Major element (wt%, loss on ignition (LOI) corrected) and trace element (ppm) composition of Aldynbulak, Uttug-Khaia, and Chingin forearc basalts

Group	Aldynbulak basalts									Uttug-Khaia basalts		
Site	Shat					Buura			Tapsa	Uttug-Khaia		
Sample	KhSh-314/2	Kh12-315/2	Kh12-316/2	KhSh-17/12	KhSh-18/12	Bur-1/14	Bur-5/14	Bur-6/14	Tp-3/2	KhU-66/12	KhU-68/12	KhU-73/12
SiO_2	45.96	49.39	46.91	48.97	49.32	50.71	49.67	49.57	50.46	51.82	51.89	49.84
TiO_2	3.99	2.17	4.07	2.13	1.35	3.18	4.47	2.18	2.02	1.44	1.92	2.44
Al_2O_3	15.04	15.47	13.30	20.76	21.52	15.05	15.44	17.09	14.99	15.20	14.47	13.10
Fe_2O_3	16.32	10.16	16.68	9.66	8.11	19.34	16.61	18.00	12.85	9.94	12.45	15.36
MnO	0.23	0.20	0.22	0.13	0.15	0.11	0.18	0.27	0.20	0.18	0.18	0.24
MgO	3.99	6.20	4.78	2.32	2.03	2.28	2.56	3.82	5.49	6.22	6.43	6.92
CaO	8.77	11.41	7.90	9.64	12.53	2.79	3.76	2.40	9.88	9.85	8.23	8.37
Na_2O	4.19	3.84	4.42	4.20	4.00	3.31	4.00	5.56	3.06	4.61	3.95	3.37
K_2O	0.95	0.93	1.30	1.93	0.89	2.63	2.61	0.89	0.80	0.62	0.33	0.13
P_2O_5	0.54	0.23	0.41	0.26	0.09	0.61	0.69	0.22	0.25	0.11	0.15	0.23
LOI	3.87	3.91	3.02	5.31	1.00	4.23	5.06	4.87	4.34	4.32	3.52	3.19
Total	100.25	99.27	100.01	100.39	98.48	101.96	100.77	101.80	100.01	99.16	100.33	100.33
Mg#	0.33	0.55	0.36	0.32	0.33	0.19	0.23	0.30	0.46	0.55	0.51	0.47
Rb	13.9	19.9	23.2	22.9	6.6	55.3	111	30.0	13.4	8.3	5.5	1.4
Sr	347	577	590	510	444	359	298	485	298	192	280	204
Y	39.6	18.1	27.8	18.5	12.9	20.2	30.5	21.3	32.1	26.1	39.4	50.1
Zr	331	143	244	131	83	250	308	117	159	73.5	120	147
Nb	41.47	14.58	32.89	20.11	11.61	38.7	46.2	15.2	13.93	1.6	2.9	5.4
Cs				0.12	0.82	1.3	2.3	1.1	0.29	0.31	0.34	0.16
Ba	683	146	133	397	239	296	319	143	746	146	58.8	28.4
La	34.82	12.10	26.67	16.58	9.58	26.3	33.3	11.5	14.28	2.4	4.9	5.8
Ce	80.82	29.30	61.04	33.91	20.59	52.6	78.0	24.0	34.91	7.7	13.9	17.3
Pr	10.38	3.89	7.85	4.36	2.76	7.0	9.8	3.6	4.65	1.4	2.3	2.8
Nd	48.90	19.30	36.87	18.64	11.89	29.9	41.1	16.2	21.06	7.8	12.3	15.1
Sm	11.30	4.82	8.38	4.30	2.67	6.7	9.4	4.2	5.11	2.8	4.1	5.1
Eu	3.60	1.71	2.84	1.51	1.17	2.0	3.0	1.4	1.82	1.1	1.5	1.6
Gd	12.37	5.55	9.10	4.34	2.60	6.3	9.3	4.8	6.76	4.0	5.8	7.3
Tb	1.73	0.81	1.25	0.63	0.43	0.89	1.3	0.77	1.06	0.69	0.96	1.2
Dy	10.61	4.89	7.57	3.97	2.56	4.5	6.9	4.4	6.48	4.5	6.3	8.1
Ho	2.01	0.91	1.44	0.72	0.47	0.76	1.2	0.9	1.35	0.94	1.4	1.7
Er	5.44	2.63	3.91	1.92	1.26	1.9	3.1	2.4	3.75	2.8	4.3	5.2
Tm	0.72	0.32	0.49	0.26	0.17	0.23	0.39	0.31	0.54	0.39	0.62	0.75
Yb	4.61	2.04	3.16	1.72	1.18	1.4	2.4	2.0	3.30	2.5	4.2	4.9
Lu	0.68	0.30	0.47	0.27	0.16	0.20	0.33	0.27	0.50	0.37	0.65	0.74
Hf	7.30	3.65	5.85	3.21	1.99	5.4	7.1	2.9	3.83	2.1	3.0	3.9
Ta	2.63	0.92	2.10	1.24	0.65	2.32	2.83	0.97	0.83	0.15	0.37	0.40
Pb	3.65	5.73	2.69			3.2	3.6	1.5	2.78	0.17	0.50	0.52
Th	3.28	1.08	2.34	1.27	0.67	2.4	3.4	1.0	1.57	0.13	0.25	0.55
U	0.96	0.40	0.66	0.34	0.25	0.47	0.76	0.27	0.58	0.48	0.16	0.21
Th_n/Yb_n	3.9	2.9	4.0	4.0	3.1	9.4	7.5	2.8	2.6	0.3	0.3	0.6
La_n/Yb_n	5.2	4.1	5.8	6.6	5.6	12.8	9.4	3.9	3.0	0.6	0.8	0.8
La_n/Nb_n	0.85	0.84	0.82	0.83	0.83	0.69	0.73	0.77	1.04	1.51	1.67	1.07

Group	Uttug-Khaia basalts		Uttug-Khaia dikes		Chingin basalts							
Site	Uttug-Khaia				Izinziul'		Koiard					S.-Tash
Sample	KhU-302	KhU-303	KhU-69/12	KhU-70/12	KI-330/3	KI-331/1	KV-7/16	KV-11/16	KK-2/16	KK-4/16	KK-5/16	KS- 09-5
SiO_2	50.15	49.60	52.29	49.70	50.10	48.72	46.72	49.28	53.61	51.79	49.46	51.72
TiO_2	2.37	2.19	1.94	2.92	1.48	1.72	2.16	1.43	1.44	1.89	2.23	1.89
Al_2O_3	13.73	13.26	17.07	18.76	14.83	14.39	19.91	14.70	13.52	13.87	14.16	14.36

(Continued)

Table 1: *Continued*

Group	Uttug-Khaia basalts		Uttug-Khaia dikes		Chingin basalts							
Site	Uttug-Khaia				Izinziul'		Koiard					S.-Tash
Sample	KhU-302	KhU-303	KhU-69/12	KhU-70/12	KI-330/3	KI-331/1	KV-7/16	KV-11/16	KK-2/16	KK-4/16	KK-5/16	KS- 09-5
Fe_2O_3	14.09	15.95	10.80	11.94	13.41	14.26	9.82	11.72	9.18	11.49	11.38	13.53
MnO	0.23	0.22	0.16	0.18	0.21	0.28	0.12	0.17	0.13	0.17	0.17	0.21
MgO	5.80	6.24	5.02	2.11	5.73	6.36	3.16	9.58	8.38	7.56	9.30	6.86
CaO	8.53	8.26	6.01	7.47	10.19	10.88	14.26	10.04	9.13	8.90	9.80	7.54
Na_2O	4.08	3.67	4.95	4.85	3.36	3.09	3.07	2.80	4.38	3.85	2.80	3.59
K_2O	0.80	0.38	1.51	1.57	0.48	0.06	0.35	0.12	0.06	0.23	0.43	0.11
P_2O_5	0.22	0.22	0.24	0.49	0.22	0.25	0.45	0.16	0.17	0.26	0.28	0.19
LOI	3.5	3.41	3.15	4.51	2.36	1.92	3.95	2.93	1.86	2.92	2.65	5.85
Total	99.61	99.57	99.90	100.62	100.15	100.38	99.14	99.38	99.27	99.83	99.66	100.3
Mg#	0.45	0.44	0.48	0.26	0.46	0.47	0.39	0.62	0.64	0.57	0.62	0.50
Rb	17.0	9.7	15.5		0.70	5.92	3.10	1.79	0.79	2.6	7.3	1.75
Sr	149	98	668		281	301	372	151	171	151	143	148
Y	39.7	40.3	28.2		27.8	26.2	49	26	25	30	32	28.5
Zr	156	137	179		130	110	133	88	98	145	174	62
Nb	5.24	4.71	6.80		7.39	4.51	10.70	5.90	6.8	12.4	14.1	6.54
Cs			0.14		0.02	0.11	0.07	0.07	0.07	0.26	0.11	1.04
Ba	1,111	1,257	140		28	155	70	34	20	115	85	54
La	6.31	7.13	9.22		9.98	8.19	17.1	7.0	7.1	11.2	13.6	7.17
Ce	18.85	19.55	24.52		24.13	20.01	37.0	15.0	16.8	26.0	31.0	17.75
Pr	3.01	3.05	3.42		3.40	2.87	5.2	2.2	2.5	3.7	4.3	2.56
Nd	17.45	17.14	15.90		17.45	14.75	24	10.3	11.4	15.6	18.5	12.85
Sm	5.80	5.50	4.33		4.67	4.12	6.3	3.0	3.2	4.3	4.9	3.86
Eu	1.99	1.82	1.47		1.44	1.42	1.94	1.43	1.11	1.12	1.14	1.32
Gd	8.64	8.22	5.05		5.92	5.32	8.3	4.1	4.1	5.1	5.8	5.41
Tb	1.40	1.34	0.81		0.91	0.83	1.36	0.7	0.7	0.85	0.97	0.90
Dy	9.61	9.31	4.80		5.93	5.48	8.6	4.4	4.5	5.4	5.8	5.87
Ho	1.99	1.96	0.99		1.23	1.14	1.67	0.9	0.93	1.1	1.17	1.23
Er	6.06	5.82	2.92		3.51	3.33	4.6	2.4	2.4	2.9	3.3	3.24
Tm	0.82	0.83	0.40		0.51	0.48	0.66	0.36	0.36	0.45	0.48	0.47
Yb	5.52	5.47	2.60		3.37	3.16	4.0	2.2	2.2	2.8	2.8	3.09
Lu	0.82	0.85	0.39		0.50	0.48	0.58	0.32	0.33	0.4	0.42	0.41
Hf	4.29	3.76	3.83		3.10	2.68	3.8	2.5	2.6	3.8	4.6	1.66
Ta	0.37	0.33	0.52		0.83	0.31	0.71	0.31	0.4	0.73	0.94	0.42
Pb	5.08	3.76	3.62		1.18	1.15						1.72
Th	0.51	0.60	1.29		0.98	0.77	1.08	0.68	0.62	1.13	1.19	0.50
U	0.84	0.49	0.48		0.43	0.38	3.3	0.31	0.17	0.34	0.37	0.14
Th_n/Yb_n	0.5	0.6	2.7		1.3	1.6	1.5	1.7	1.5	2.2	2.4	0.9
La_n/Yb_n	0.8	0.9	2.4		1.8	2.0	3.0	2.2	2.2	2.8	3.4	1.6
La_n/Nb_n	1.22	1.53	1.37		1.84	1.37	1.61	1.20	1.05	0.91	0.97	1.11

Group	Chingin basalts								
Site	Tlangara		Kopsek					Koiard	
Sample	KT- 317/3	KT-317/4	KKp-1/12	KKp -2/12	KKp -4/12	KKp -7/12	KKp -8/12	KK-17/16*	KK-18/16*
SiO_2	50.43	47.44	51.68	48.05	45.96	48.96	49.28	47.89	48.92
TiO_2	1.97	1.86	1.58	1.65	1.95	1.71	2.28	2.33	3.05
Al_2O_3	16.73	15.46	14.88	15.82	16.60	14.46	17.84	15.14	14.08
Fe_2O_3	11.71	12.41	10.75	13.15	13.24	11.05	10.21	12.53	13.60
MnO	0.15	0.19	0.16	0.20	0.20	0.18	0.14	0.16	0.18
MgO	7.06	8.69	6.11	6.67	8.20	6.39	4.50	5.06	4.28
CaO	7.18	11.35	9.90	11.05	11.16	15.21	11.78	11.79	10.33

(Continued)

Table 1: *Continued*

Group	Chingin basalts								
Site	Tlangara		Kopsek					Koiard	
Sample	KT- 317/3	KT-317/4	KKp-1/12	KKp -2/12	KKp -4/12	KKp -7/12	KKp -8/12	KK-17/16*	KK-18/16*
Na_2O	4.53	2.33	4.66	2.64	2.54	1.82	3.51	4.74	4.78
K_2O	0.04	0.08	0.17	0.61	0.02	0.03	0.17	0.07	0.28
P_2O_5	0.20	0.19	0.11	0.16	0.14	0.18	0.28	0.30	0.49
LOI	4.06	3.97	2.65	2.36	3.12	2.34	2.58	5.46	4.64
Total	100.29	100.29	99.41	99.45	99.39	99.35	99.41	99.73	99.58
Mg#	0.58	0.46	0.53	0.50	0.55	0.53	0.47	0.44	0.38
Rb	0.33	0.78	1.60	8.93	0.32	0.21	1.69	0.82	1.96
Sr	241	420	233	272	685	982	479	175	214
Y	24.3	24.6	29.9	35.9	25.5	20.6	27.1	35.5	56.2
Zr	161	141	97	121	124	116	154	153	256
Nb	8.72	7.36	5.82	7.66	6.41	5.09	18.66	11.83	19.3
Cs	0.06	0.09	0.32	0.61	0.18	0.12	0.64	0.07	0.11
Ba	49	144	90	140	25	14	95	78.1	88.6
La	6.49	7.54	6.06	8.47	7.63	6.66	15.01	12.9	17.86
Ce	18.13	19.89	15.51	21.05	20.38	18.15	34.23	29.17	42.53
Pr	2.76	2.92	2.24	2.91	2.98	2.64	4.62	4.08	6.05
Nd	14.40	14.66	11.59	14.00	14.49	12.44	20.99	18.72	27.55
Sm	4.16	4.07	3.66	4.32	4.10	3.68	5.31	5.17	7.38
Eu	1.43	1.62	1.17	1.71	1.40	1.17	1.92	1.52	2.27
Gd	4.97	5.01	4.48	5.28	4.67	3.96	5.53	6.37	9.32
Tb	0.88	0.86	0.78	0.92	0.81	0.63	0.86	1.02	1.6
Dy	5.38	5.37	5.60	6.47	5.13	4.25	5.25	6.27	9.86
Ho	1.09	1.07	1.20	1.40	1.00	0.84	1.00	1.25	2.03
Er	2.93	2.91	3.47	4.04	2.90	2.33	2.76	3.61	5.58
Tm	0.39	0.39	0.49	0.60	0.43	0.33	0.39	0.54	0.80
Yb	2.34	2.35	3.13	4.00	2.56	2.01	2.50	3.18	5.10
Lu	0.29	0.31	0.47	0.60	0.37	0.30	0.35	0.46	0.74
Hf	1.76	1.25	2.71	3.06	3.15	2.92	3.55	4.12	6.18
Ta	0.53	0.33	0.37	0.49	0.43	0.37	1.17	0.74	1.19
Pb	2.23	0.80							
Th	0.47	0.41	0.67	0.99	0.46	0.21	1.27	1.19	1.56
U	0.19	0.14	0.81	0.34	0.19	0.16	0.47	0.34	0.57
Th_n/Yb_n	1.1	0.9	1.2	1.3	1.0	0.6	2.8	2.0	1.7
La_n/Yb_n	1.9	2.2	1.3	1.4	2.0	2.3	4.1	2.8	2.4
La_n/Nb_n	0.75	1.03	1.05	1.12	1.20	1.32	0.81	0.83	0.83

Note. * – basalts from the Chingin "Upper Subformation" (late Chingin basalts).
Mg# = 100 * (MgO/40.3)/((MgO/40.3) + (FeO*0.9)/71.85)).

basalts (Figure 7b–d). On the discrimination diagram in the study by Meschede [71], they fall in the field on N-MORB and take an intermediate position between N-MORB and volcanic arc basalts on the diagram in the study by Condie [70] (Figure 9a and b). Most samples are plotted as N-MORB in Tb*3–Th–Ta*2 ternary diagram (after [74]); one sample, however, falls in the field of forearc/back-arc basalts (Figure 9c). On spider diagrams (Figure 8), the samples broadly follow the trend of N- and E-MORBs. A negative Nb anomaly is present, but not well defined (Figure 8d). Elemental ratios of La_n/Yb_n = 0.6–0.9 and Th_n/Yb_n = 0.3–0.6 (Table 1) are similar to that of N-MORB: La_n/Yb_n = 0.6 and Th_n/Yb_n = 0.2 [72], but the Uttug-Khaia samples show in general an increased and unusual trace element concentration compared to average N-MORBs (Figure 8c and d).

Chingin basalts. The petrochemical composition (after [69]) of the Chingin basalts corresponds mainly to basalt (28 samples), less often basaltic andesite (4 samples), and in one case to trachybasalt (Figure 7a). A large scatter of the magnesium content data points are recognized as

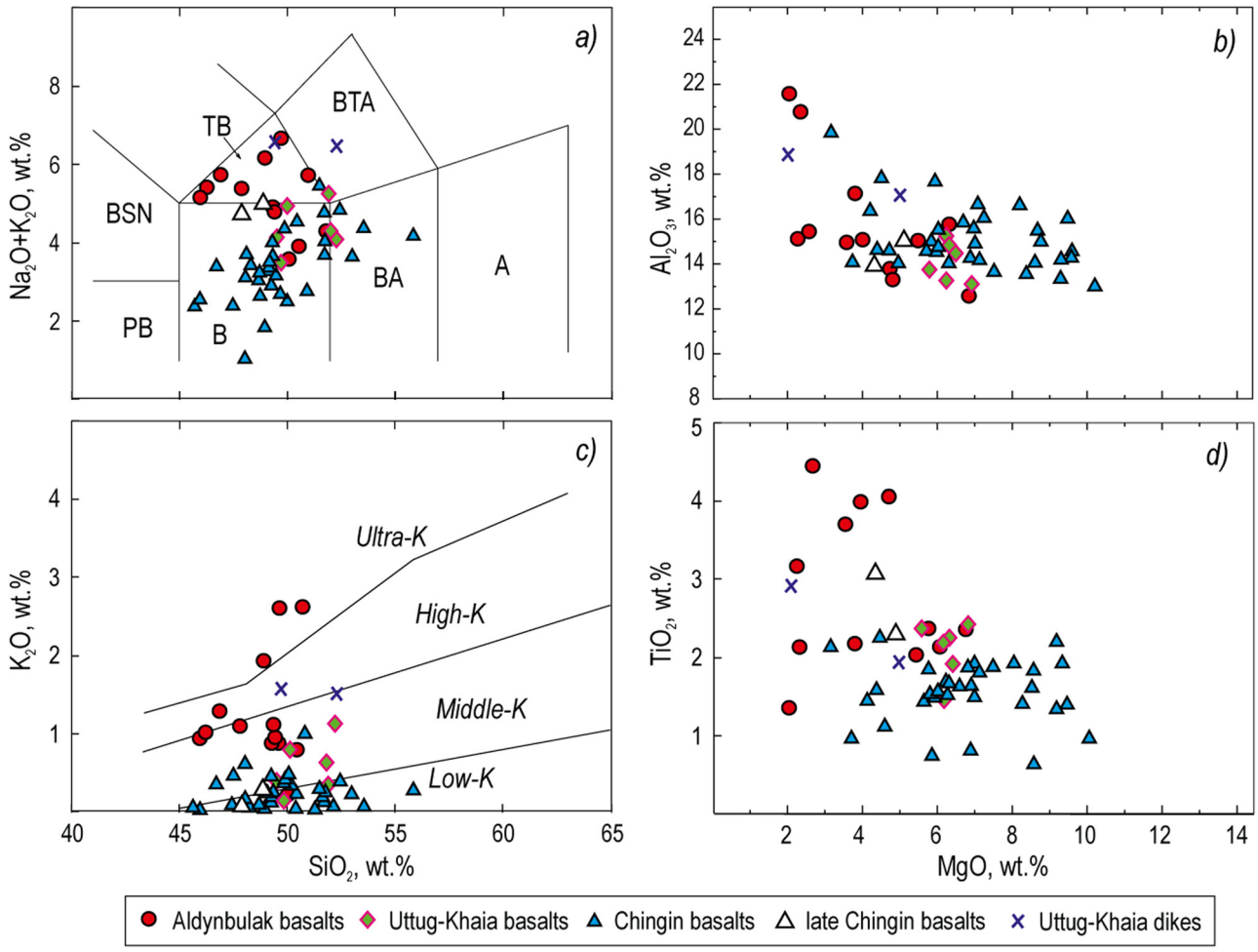

Figure 7: Petrochemical diagrams of major elements for the studied forearc basalts. (a) $Na_2O + K_2O$ vs SiO_2 [69]: A – andesite, B – basalt, BA – basaltic andesite, BSN – basanite, BTA – basaltic trachyandesite, PB – picrobasalt, TB – trachybasalt; (b) Al_2O_3 vs MgO; (c) K_2O vs SiO_2 [104]; and (d) TiO_2 vs MgO. Here and further: "Late Chingin" refers to the "Upper Subformation." Data from Table 1 and supplementary Table S1 were used for the charts in (a)–(d). For additional information the reader is referred to Table S1.

MgO = 3.2–10.2 wt% (Mg# = 0.35–0.64) which is also in overall higher compared to the Aldynbulak (MgO = 2.0–6.8 wt% and Mg# = 0.19–0.55) and Uttug-Khaia (MgO = 5.8–6.9 wt% and Mg# = 0.44–0.55) samples (Figure 7b and c). The TiO_2 = 0.6–3.1 and K_2O = 0.02–0.99 wt% values are noticeably lower than in the Aldynbulak basalts (Figure 7). The basalts sampled from the upper and lower subformations of the Chingin Formation exhibit an almost identical composition (Figures 8 and 9), even though a high content of TiO_2 = 3.05 wt% and the highest concentration of trace elements was found in the upper subformation (sample KK-18/16*) (Table 1, Figures (6e and f) and (7d)). On the Nb*2–Zr/4–Y (after [71]) and Nb/Th vs Zr/Nb (after [70]) diagrams, the Chingin samples occupy the compositional fields of N-MORB and intraplate tholeiites and ocean plateau basalts, respectively (Figure 9a and b). However, on the Tb*3–Th–Ta*2 ternary diagram (after [74]), the Chingin samples are plotted mainly in the field of E-MORB and ocean island basalts. Three samples are plotted in the field of forearc/back-arc basalts and two samples are even of continental tholeiitic composition (Figure 9c). The E-MORB-like composition also reflected in the trace element ratios La_n/Yb_n = 1.3–4.1 and Th_n/Yb_n = 0.6–2.8 of the Chingin basalts are similar to E-MORBs: La_n/Yb_n = 2.9 and Th_n/Yb_n = 2.2 and T-MORBs (transitional mid-ocean ridge basalts): La_n/Yb_n = 1.1 and Th_n/Yb_n = 0.7 [73] (Table 1) and in the spider diagram (Figure 8e and f).

Uttug-Khaia dikes. The dikes that cut through the Uttug-Khaia Formation basalts (samples KhU-69/12 and KhU-70/12) are trachybasalts and basaltic trachyandesites (Table 1, Figure 7a). These samples have high alumina (Al_2O_3 = 17.1 and 18.8 wt%), moderate and low-magnesium (MgO = 5.0 and 2.1 wt%, Mg# = 0.48 and 0.26), high titanium (TiO_2 = 1.94 and 2.92 wt%), and high potassium (K_2O = 1.51 and 1.57 wt%) contents (Figure 7). Only one sample was available for further trace element

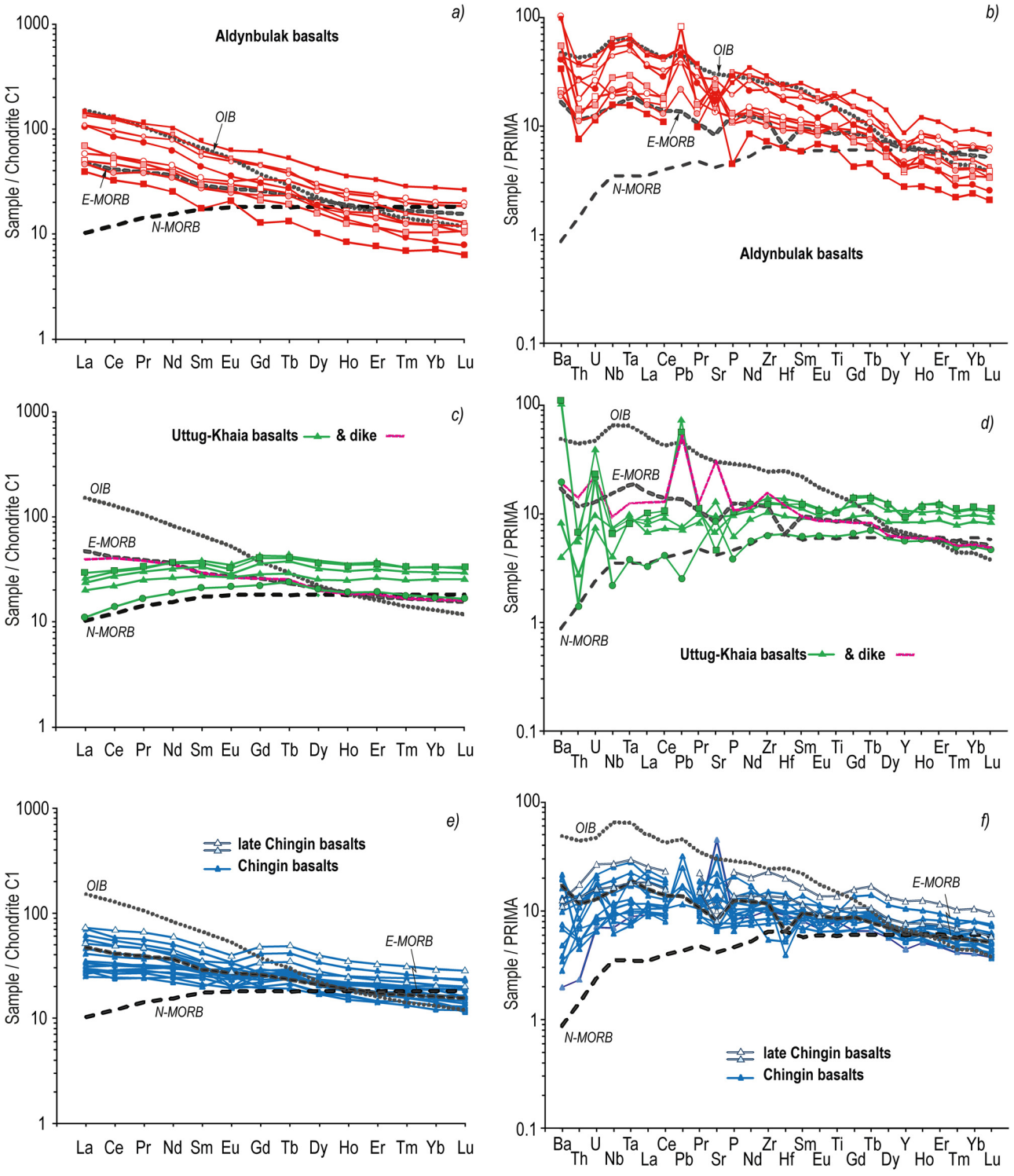

Figure 8: Spider diagrams of chondrite- and primitive mantle-normalized [72] trace element patterns. (a) and (b) Aldynbulak basalts; (c) and (d) Uttug-Khaia basalts and dike KhU-69/12; and (e) and (f) – Chingin basalts and late Chingin basalts.

analytics (KhU-69/12). On the diagrams after Condie [70] and Meschede [71], this sample is plotted in the field of volcanic-arc basalts or intraplate tholeiites (Figure 9a and b). On the Tb*3–Th–Ta*2 ternary diagram (Figure 9c) (after [74]), this sample, however, is plotted in the field of continental tholeiites. On the spidergrams (Figure 8c and d) and according

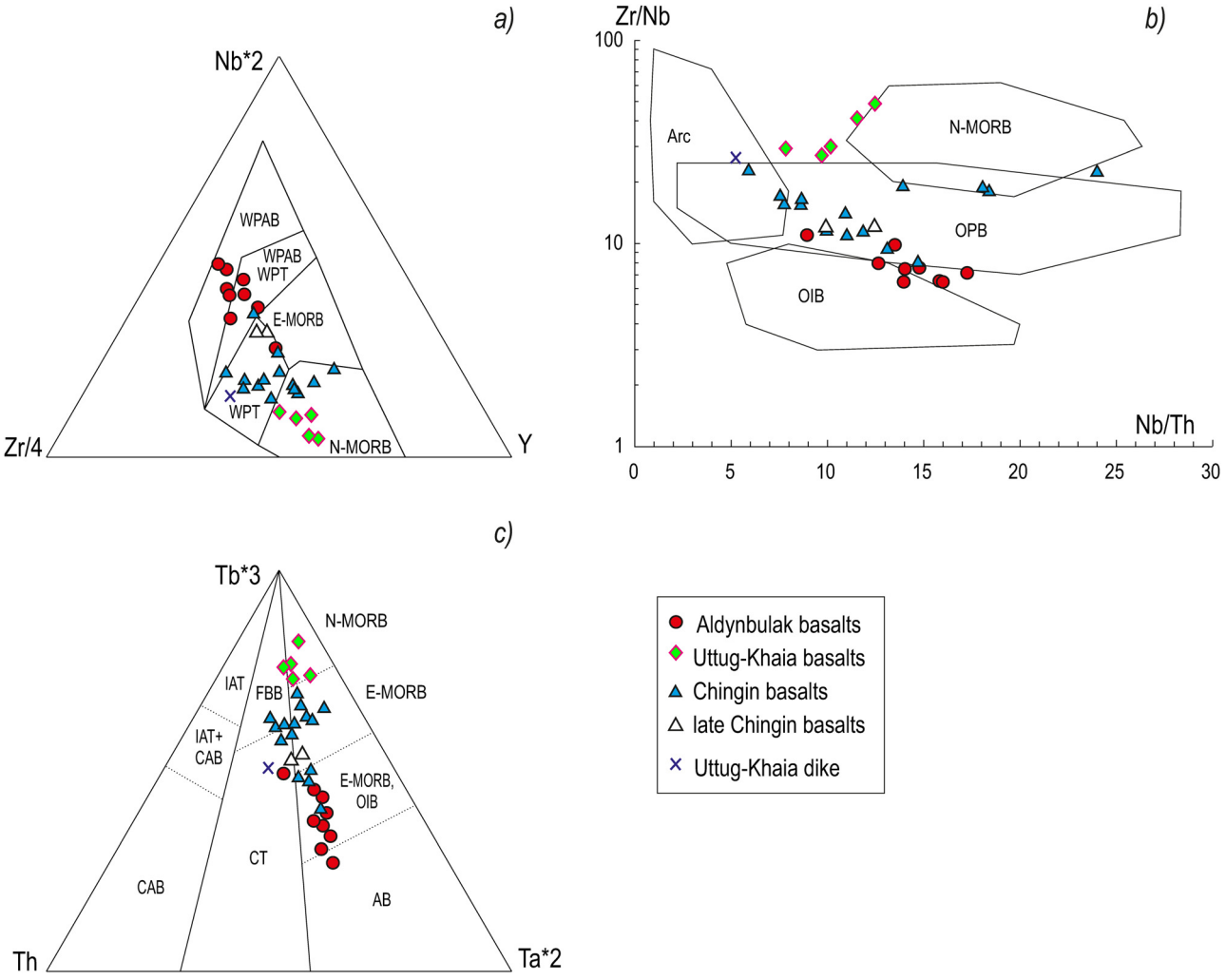

Figure 9: Discriminant diagrams for the basalt and dike samples. (a) Nb*2 – Zr/4 – Y after [71]; (b) Zr/Nb vs Nb/Th after [70]; and (c) Tb*3–Th–Ta*2 after [74]. Compositional fields of all diagrams: AB – alkaline basalts, Arc – volcanic-arc basalts, CAB – calc-alkaline basalts, CT – continental tholeiites, FBB – forearc and back-arc basalts, IAT – island arc tholeiites, N- and E-MORB – normal and enriched mid-oceanic ridge basalts, OPB – oceanic plateau basalts, OIB – oceanic island basalts, WPAB – intraplate alkaline basalts, WPT – intraplate tholeiites.

to La_n/Yb_n = 2.4 and Th_n/Yb_n = 2.7 ratios (Table 1), the dike sample KhU-69/12 is close to the composition of E-MORB (La_n/Yb_n = 2.9 and Th_n/Yb_n = 2.2 [73]). It was noted that the composition of the dike shows a similar trace element pattern and composition to the Chingin basalt samples (Figure 8d and f).

4.2.2 Sm–Nd isotopic composition and assessment of basalt magma sources

To estimate the phase composition of mantle protoliths and the degrees of their partial melting, the element ratios of Lu/Hf vs La/Sm (Figure 10a) (after [75]), $(La/Sm)_n$ vs Zr/Nb (after [76–78] (Figure 10b), and Y/Nb vs Zr/Nb (Figure 10c) (after [77,78]) were plotted.

The Aldynbulak basalts plot predominantly in the intermediate region of the two peridotite phases, both showing low degrees of partial melting (Figure 10a). These basalts are further characterized by relatively low positive values of initial ε_{Nd} (T) = +3.7 to +5.7 (Table 2), which is probably due to the presence of a recycled primitive mantle component in their source [79]. Considering the OIB + E-MORB-like composition of the Aldynbulak basalts, it is likely that an enriched deep mantle source was of primary importance in their petrogenesis. This is also seen on the $(La/Sm)_n$ vs Zr/Nb and Y/Nb vs Zr/Nb diagrams (Figure 10b and c) on which the samples were plotted close to the field of E-MORBs. Note that the Tp-3/2 sample with the highest Lu/Hf ratio = 0.13 is linked with the highest $\varepsilon_{Nd}(T)$ = +5.7 value among the Aldynbulak basalts (Table 2, Figure 10a).

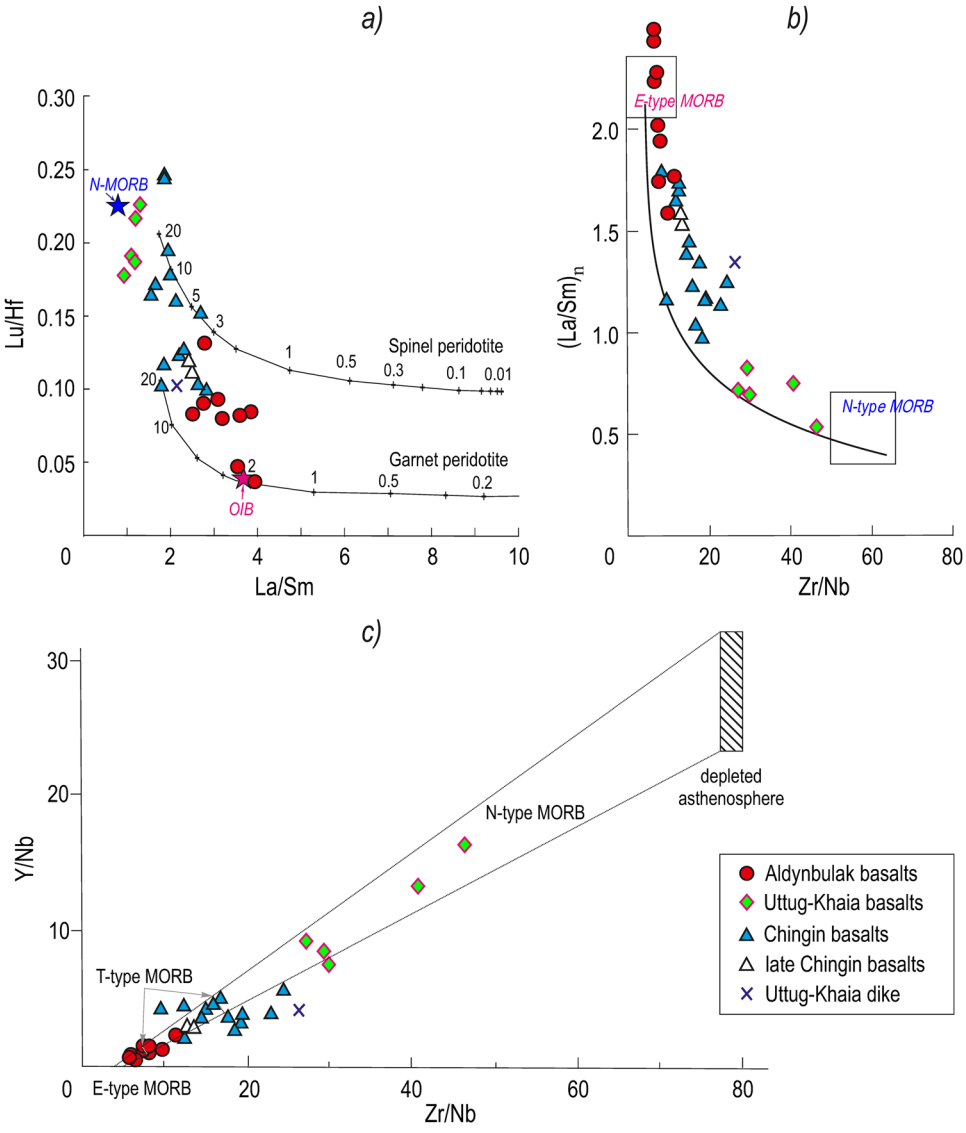

Figure 10: Diagrams reflecting the degree of partial melting and source. (a) Lu/Hf vs La/Sm after [75], (b) $(La/Sm)_n$ vs Zr/Nb after [76–78], and (c) Y/Nb vs Zr/Nb after [77,78].

The Chingin basalts are characterized by relatively high positive $\varepsilon_{Nd}(T)$ = +6.7 to +8.3 values, indicating a larger contribution of juvenile mantle components in the source [80]. The ε_{Nd} values of the Chingin basalts are also close to those of the depleted mantle of the respective age $\varepsilon_{Nd}(0.57)$ = +8.8 [81]. Possibly, the Chingin samples represent a mixture of melts created at high degrees of partial melting of garnet and spinel peridotite (Figure 10a). The $(La/Sm)_n$ vs Zr/Nb and Y/Nb vs Zr/Nb diagrams (Figure 10b and c) place the Chingin basalts between E- and T-MORBs, indicating multiple, including deeply rooted, mantle sources. Also note that the sample KKp-8-12 shows one of the lowest Lu/Hf ratios = 0.10 and the lowest $\varepsilon_{Nd}(T)$ = +6.7 value of the Chingin basalt samples (Table 2).

The Uttug-Khaia basalts are typified by an extraordinary composition. According to the Lu/Hf vs La/Sm diagram, they were formed at high degrees of partial melting of spinel peridotite (Figure 10a), which is consistent with the N-MORB-like distribution of trace elements (Figures 8c and d, 9, and 10b and c). However, the ε_{Nd} (T) = +6.3 value is lower and the concentrations of Ti and K are noticeably higher than in the E + T-MORB-like Chingin basalts (Table 2, Figure 7). This may suggest that the Aldynbulak basalts also influenced the largely N-MORB-like melt of the Uttug-Khaia basalts.

The E-MORB-like Uttug-Khaia dike (Figure 8c), which is derived from a deep mantle source in the garnet stability zone (Figure 10a), is consistent with relatively high

Table 2: Sm-Nd isotopic data for the Sayan-Tuvan forearc zone rock samples

No.	Sample number	Age, (Ma)	(Sm), (ppm)	(Nd), (ppm)	$^{147}Sm/^{144}Nd$	$^{143}Nd/^{144}Nd \pm 2\sigma$	$\varepsilon_{Nd}(T)$	T_{Nd} (DM), (Ma)
Aldynbulak basalts								
1	KhSh-314/2	578	8.93	38.85	0.138869	0.512628 ± 27	4.1	1,066
2	KhSh-315/2	578	4.14	16.52	0.151552	0.512698 ± 27	4.5	
3	KhSh-316/2	578	7.08	31.17	0.137277	0.512601 ± 38	3.7	1,098
4	KhSh-17-12	578	4.11	18.02	0.137780	0.512630 ± 11	4.2	1,047
5	Bur-5/14	578	9.57	44.0	0.13150	0.512618 ± 10	4.5	939
6	Tp-3/2	578	5.13	19.49	0.159023	0.512785 ± 7	5.7	
Uttug-Khaia basalts								
7	KhU-302	578	4.99	14.83	0.203288	0.512987 ± 33	6.3	
Uttug-Khaia dike								
8	KhU-69/12	578	5.11	19.1	0.16206	0.512906 ± 10	7.8	
Chingin basalts								
9	KT-317/4	578	4.17	14.67	0.171707	0.512929 ± 21	7.5	
10	KKp-7-12	578	3.41	12.51	0.164612	0.512941 ± 11	8.3	
11	KKp-8-12	578	5.00	20.37	0.148229	0.512797 ± 10	6.7	
Dzhebash Group (metamorphic fine-grained volcano-sedimentary shale)								
12	KKp-5-12	520	5.60	33.09	0.102291	0.512389 ± 13	1.2	1,043

concentrations of titanium, potassium, and alkaline elements (Table 1, Figure 5). The high positive $\varepsilon_{Nd}(T)$ = +7.8 value (Table 2), usually characteristic for the depleted mantle [80], hints a predominantly juvenile magma source for the Uttug-Khaia dike. The combination of the trace element content and Sm-Nd isotopic composition presumably results from the chemical and isotopic heterogeneity of the deep mantle reservoir that is associated with the subduction and recycling of oceanic crust and sediments [79].

The Sm-Nd isotopic composition of a fine-grained volcano-sedimentary rock sample from the Dzhebash subzone was also studied: $\varepsilon_{Nd}(T)$ = +1.2 and T_{Nd}(DM) = 1,043 Ma (Table 2). A low positive value of initial ε_{Nd} in this sample may indicate mixing of late Mesoproterozoic–early Neoproterozoic and early Paleozoic isotopic provinces [81].

5 Discussion

5.1 Accretion vs non-accretion

The geochemical analyses of basalts from the Sayan-Tuvan forearc zone identified four different groups. The first two groups are the enriched OIB + E–MORB-like Aldynbulak basalts (Shat, Buura, and Tapsa sites) and N-MORB-like Uttug-Khaia basalts (Uttug-Khaia site) of the Khemchik-Tapsa forearc subzone. The third group is the E + T-MORB-like Chingin basalts of the Kurtushiba forearc subzone. Based on the similarity of the chemical composition, the Uttug-Khaia dikes (samples KhU-69/12 and KhU-70/12) are likely part of the Chingin Formation which cut through the Uttug-Khaia basalts. The fourth group of basalts comprises altered green- and blueschists of the Dzhebash Group located in the Dzhebash accretionary subzone [22] whose ocean plateau origin has been described in previous studies (Section 2.1).

If we followed the "accretionary model," it would be possible to argue that our results theoretically suggest that oceanic seamounts or lava plateaus (Aldynbulak, Uttug-Khaia, and Chingin Formations), and primitive arc and inter-arc or back-arc basin rocks (Kurtushiba and Khemchik ophiolites) were successively accreted to a suture zone related to the larger Tannuola-Khamsara terrane complex during the early Paleozoic without sharing a common origin. Previous authors described that the Kurtushiba subzone contains different complexes of oceanic ophiolites, oceanic islands, and plateaus with a sedimentary cover [14]. Volkova et al. [22] re-studied the Chingin Formation in the Kurtushiba zone and found differences in the geochemical properties of the basalts. The Chingin was divided into the Kurtushibinsky Formation (oceanic lava plateau) and the Verkhnekoyardsky Formation (basalt and sediment bearing part of the ophiolites). The Kurtshibinsky Formation basalts may just represent a non-metamorphic analog of the Dzhebash Group basalts [22]. Their data suggest that the basalts of the Kurtushibinsky Formation formed an oceanic plateau that was accreted to the forearc/accretionary zone but avoided subduction metamorphism in contrast to the Dzhebash Group [22], generally favoring an accretional origin of the Kurtushiba zone ophiolitic suites. This is in consensus with the prevailing view that the Dzhebash, Kurtushiba, and Khemchik-Tapsa subzones represent accretionary suture-like

zones [14,25,43] and the rock units found therein may not share a common geodynamic development.

Contrarily, stratigraphic and petrologic observations imply that alternative models are also feasible. The Chingin Formation as a whole is traditionally considered part of the Kurtushiba ophiolites [44] and the Chingin basalts gradually turn into gabbro at the Kyzyr-Burlyuk site which is part of the Kurtushiba ophiolite complex [82]. Boninites are not only present among the dikes of the Kurtushiba ophiolites [57], but also among the Chingin basalts (Section 2.2). Boninites are important marker rocks that commonly form in oceanic subduction settings [83] and an association with forearc magmatism and suprasubduction zone ophiolites has been stressed [33,34]. However, boninites may also form in different environments like back-arc settings [33,83], which complicates an unambiguous interpretation, especially since boninites can be associated with the basement of arcs [34]. Three datapoints of the Chingin samples fall in the field of forearc/back-arc basalts on the Tb*3–Th–Ta*2 diagram (Figure 9c) and the Kurtushiba ophiolite rocks are largely plotted in the field of forearc plateau basalts [59], favoring a forearc magmatic setting for the Chingin basalts and Kurtushiba ophiolite.

The Aldynbulak and the Uttug-Khaia formations are considered part of the Khemchik ophiolites [42,51]. Even though boninites have not been reported, one measurement of the Uttug-Khaia basalts falls in the field of forearc/back-arc basalts (Figure 9c) and a forearc affinity has been shown for the Khemchik ophiolitic rocks [59]. In addition to the forearc affinity of the studied sections, several other factors support that these were formed in a coherent subduction setting:

The ophiolitic strata is 578 Ma old [37] which is nearly the same age as the arc granites of the Tannuola-Khamsara system (572 Ma) [39]. An arc origin is favored by Rudnev et al. and the negative Nb-Ta anomaly of the granitic rocks suggests a subduction-related origin, at least for the earlier granitic suites [38,39]. Also, the ophiolitic sequences from the Kurtushiba and Khemchik subzones have geochemical similarities with the “normal” island arc complexes of the Tannuola-Khamsara island arc (Section 2.4.3).

The Agardag back-arc subzone is of similar age compared to the Khemchik and Kurtushiba ophiolite systems [37,64] and also shows geochemical subduction, back-arc or even suprasubduction origin affinities [32,63].

Possible late Ediacaran to earliest and early Cambrian sedimentary strata, overlying and partially also overlapping the different ophiolitic and basaltic units, frequently contain lithofacies like conglomerates or olistoliths with recycled fragments of exactly those underlying mafic-ultramafic rocks (of the Kurtushiba and Khemchik(-Tapsa) subzones) [35,36]. Ophiolitic units preserved in olistostromes and serpentinic mélange zones can be commonly encountered in subduction initiation and active forearc basin settings [84–88]. Even though middle to late Ediacaran and earliest Cambrian fossil evidence is scarce, paleobiogeographic studies of early Cambrian fossils show that the different terranes of the Sayan-Tuvan forearc zone were part of a large, yet, local basin at least starting with Cambrian Age 3 (~Atdabanian) [89,90].

The basalt dikes within the Uttug-Khaia Formation are geochemically similar to the Chingin basalts (Figure 6c–f), presumably implying that the Chingin Formation is younger or at least time-equal to the Uttug-Khaia Formation and was generated spatially close to the Uttug-Khaia basalts.

Thus, an alternative approach is required to explain the occurrence of the various geochemically different igneous units. We argue that the basalts and paleospreading complexes found in the Sayan-Tuvan forearc zone accretionary complexes, among tectonic slivers in the forearc basin and molasse deposits and close to the island arc do share a stratigraphic and geochemical co-genetic connection and are linked with the formation of the Tannuola-Khamsara island arc. Our model does not stand in contrast with the presumption that some part of the forearc basalts and suprasubduction complexes (Dzhebash Group) were incorporated into an accretionary wedge during the Cambrian and early Ordovician but given the observations in the field and geochemical results, we argue that there may have been a preceding stage in which the basalts of the Aldynbulak, Chingin, and Uttug-Khaia formations were formed – namely – in a forearc spreading setting.

5.2 Subduction initiation and formation of proto-arc – forearc crust: Conclusions from Mesozoic and recent examples

Initial phases of volcanism in the intraoceanic Izu–Bonin–Mariana (IBM) forearcs developed nearly synchronously in the middle to late Eocene over a zone up to 300 km wide and thousands of kilometers in length, with the initial magmatic arc activity occupying a much broader zone than later volcanic activity [3,91]. Potential scenarios for the origins of the Mariana forearc basalts have been proposed including volcanism at a spreading center before subduction initiation

or igneous processes during near-trench spreading after subduction began [92,93]. Whattam and Stern [12] concluded that the earliest stages of subduction involved decompression melting of a fertile, lherzolitic, asthenospheric source to form early MORB-like rocks as seen in the lowermost sections of Tethyan ophiolites and the IBM forearc. The study of the Izu-Bonin forearc basalts showed that they formed in two stages, with early melts of the garnet fields being extracted before the later melts of the spinel field [13]. At the same time, the melts of the IBM forearc basalts have a depleted nature, which is a regional characteristic that originated well prior to the time of subduction initiation [94].

In another example of subduction initiation, studies of Jurassic ophiolites from Albania showed that these rocks formed in a setting where high Ti, low Ti, and very low Ti magmatism coexisted either spatially or temporally [9], similar to the different basalts from the Sayan-Tuvan forearc zone (Figure 7d).

Trends in the trace element patterns of the Sayan-Tuvan forearc basalts (especially with the herein studied Aldynbulak samples) are highly comparable with data reported from the Cretaceous Bursa suprasubduction zone ophiolite located in northwestern Turkey [95]. At Bursa, amphibolites form the metamorphic sole (96 Ma) of the ophiolites and are enriched in light rare earth elements (LREE), large-ionic lithophilic elements (LILE), and have an E-MORB-like composition (which was likely the geochemical composition of the basaltic protoliths). The later complex of the mafic dikes with an age of about 90 million years is depleted in LREE and slightly enriched in LILE with a MORB-like mantle source similar to the earliest forearc basalts in the IBM suprasubduction system [94] (Uttug-Khaia and Chingin basalts).

Dilek and Furnes [11] demonstrated in a review article that the initiation of subduction is followed by a rapid slab rollback leading to extension and sea floor spreading in the upper plate. In the earliest phase of subduction initiation, magma is first generated by decompression melting of a deep and fertile lherzolitic mantle and produces the earliest crustal rocks with MORB-like composition. Fluids derived from the subducted slab have little influence on melt evolution at this early stage. The subsequent phases of melting, however, are strongly influenced by slab dehydration and related mantle metasomatism, melting of subducting sediments, repeated episodes of partial melting of metasomatized peridotites, and mixing of highly enriched liquids from the lower fertile source with refractory melts in the melt column beneath the extending protoarc–forearc region [11] (Figure 11a for overview of processes).

5.3 Development of the Sayan-Tuvan forearc zone

We propose a multi-step evolution of the Sayan-Tuvan forearc zone (Figure 11a–d) applying the models and considerations brought forward by Shervais and Choi [27], Metcalf and Shervais [96], and especially Dilek and Furnes [11]. Figure 11 combines the available tectonostratigraphic, geological, geochemical, and geochronological data.

5.3.1 First stage (580–578 Ma ago)

During the first stage (Figure 11b), about 580–578 Ma ago, the initiation of subduction causes decompression melting of the mantle from garnet peridotite at low degrees of partial melting, which led to the generation of basalts with OIB + E–MORB-like composition (Aldynbulak and Kuskunnug basalts, see Section 2.4), that likely arose as an intra oceanic plateau basalt structure at some distance from the newly-forming trench (Figure 11b), assumed from the stratigraphic and structural position. Yang et al. [32] indicated a “suprasubduction and plume”-type setting for the Kurtushiba and Shatskii massifs; however, no unambiguous evidence for plume magmatism was found in this study.

5.3.2 Second stage (578–572 Ma ago)

About 578–572 Ma ago (Figure 11c), a distinct slab rollback was accompanied by several suprasubduction spreading centers (Figure 11c), where mainly decompression (+fluid flux) melting of the depleted mantle took place. Paleospreading complexes of the Khemchik (~578 Ma [37]) and Kurtushiba ophiolites were formed during these intervals and possibly, the formation of Uttug-Khaia basalts began. There was likely an additional spreading center close to the Ondum subzone, which evolved into island arc magmatism in the following stages (Figure 11d and e). This is indicated by the earliest plagiogranites of the Ondum island arc subzone with an age of 572–562 Ma and an N-MORB-like distribution of trace element values [38,39]. Data on the age of the Agardag ophiolites (Section 2.4.4) indicate that they also began to form during this period. The suprasubduction crust probably consisted not only of newly formed oceanic crust, but also included remnants of older MOR-type oceanic rocks, which were gradually replaced by suprasubduction melts (primary MOR-type crust was found in the parts of Kurtushiba ophiolites that were presumably located closest to the trench, see Section 2.4).

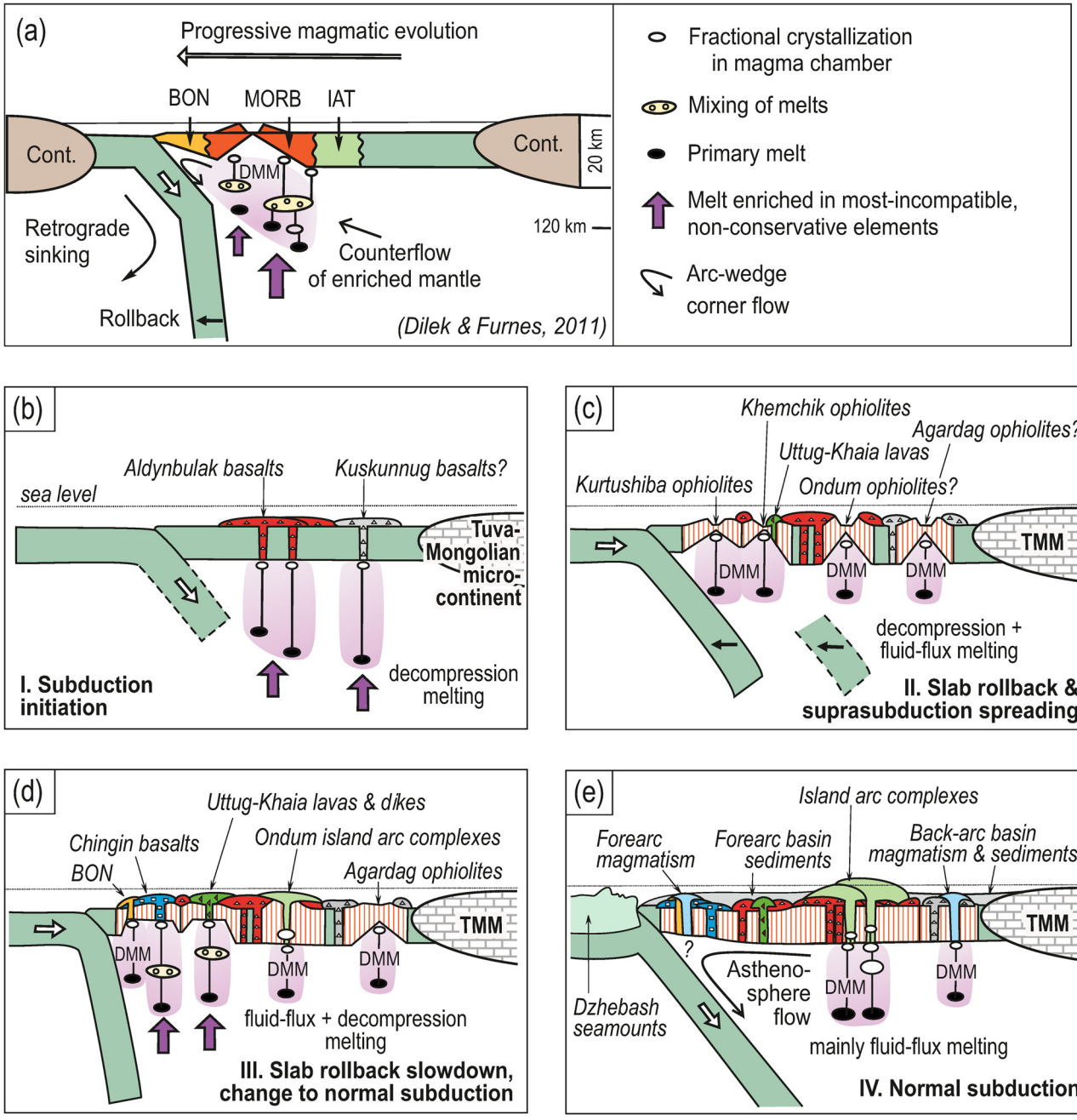

Figure 11: Suggested formation model of suprasubduction complexes during the initial stages of subduction. The reader is referred to the text for a detailed discussion of the figure. (a) A generalized model of the formation of suprasubduction ophiolites (modified from Figure 7-B1 from [11]. Used with permission. Copyright Geological Society of America.); (b)–(e) Assumed geodynamic evolution of the individual stages of the Tannuola-Khamsara island arc subduction zone; (b) The first stage shows the initiation of subduction and decompression melting of the enriched mantle at low degrees of partial melting under the thick oceanic crust of the MOR–type. 580–578 Ma marks the estimated onset of subductions processes, assumed from the age of the Shatskii ophiolite massif (~578 Ma [37]); (c) The second stage displays the slab rollback and suprasubduction spreading, decompression, and fluid-flux melting of the depleted mantle and the formation of forearc paleospreading complexes, presumable gradual magmatic replacement of the older MOR-type crust, possibly also the genesis of the proto-arc Ondum ophiolites and island arc granites [38,39], and the supposed beginning of the formation of Uttug-Khaia basalts and Agardag ophiolites; (d) The slab rollback slows down and the transition to normal subduction begins, in the forearc zone decompression melting of enriched and depleted mantles sources at high degrees of partial melting and mixing of melts leads to the continued formation of the Uttug-Khaia basalts and Chingin basalt magmas under the newly formed, relatively thin, forearc oceanic crust. Close to the forearc zone, the Ondum island -arc plagiogranites develop (with an age of ~572–562 Ma [38,39]) and in the back-arc zone, decompression and fluid flux melting of the depleted mantle, create the Agardag back-arc paleospreading complexes with an age of ca. 580–574 Ma [63,64] (see 2.d.4); (e) A normal subduction regime is established during the last phase of the subduction zone development. 538 Ma is assumed to represent the age of late forearc magmatic activity; back-arc magmatism continued during that time as well. MORB – mid-oceanic ridge basalts, IAT – island arc tholeiites, BON – boninites, DMM – depleted metasomatized mantle.

5.3.3 Third stage (572–562 Ma ago)

The third stage (Figure 11d), at about 572–562 Ma, marks the slab rollback slowdown and transition to normal subduction. During this stage, the formation of forearc complexes continues, and the first island arc and back-arc complexes are established. The basalt lavas that now form the dominant variants are the mixing product of different enriched and depleted melts: N-MORB-like Uttug-Khaia basalts, E-MORB-like Uttug-Khaia dikes, and the E + T-MORB-like Chingin basalts. Apparently, the introduction of boninites also took place at the same time (Figure 11d) in the Kurtushiba zone Section 5.3.5.

The third stage probably also records the transition from predominantly decompression melting to predominantly fluid-flux melting of the newly formed suprasubduction crust. Possibly, the Uttug-Khaia and Chingin basalts were formed during the final stages of a fading forearc spreading zone, while the first island arc complexes, in particular, Ondum plagiogranites, were formed closely to the suprasubduction complexes. The growth of the Agardag ophiolites with an age of ~570–546 Ma [63] may also be associated with decompression and fluid-flux melting of the depleted mantle in the back-arc spreading center [31,65]. The Agardag zone, as possible suprasubduction ophiolite [32], implies that the basalts and ophiolites evolved in multiple episodes during that time (Kuskunnug basalts and Agardag spreading complexes, see Section 2.4.4, Figure 11b and d)).

It is notable to mention that the duration of these three stages is roughly comparable to the timescales and duration of subduction initiation and subsequent evolution of the IBM system. There, the first basaltic magmatism at subduction initiation was produced by decompression melting of the mantle 52–51 Ma before present. The change in flux melting and boninitic volcanism took about 2–4 million years and the change from fluid-flux melting in counter-flowing mantle to “normal” arc magmatism is assumed to have taken 7–8 million years [97].

5.3.4 Fourth stage (562–538 Ma ago)

In the last stage, at about 562–538 Ma (Figure 11e) before present, a normal subduction regime is established. At about the same time, plagiogranite-plagiorhyolite island arc magmatism of the Ondum subzone is accompanied by basalt-andesite-rhyolite and gabbroid island arc magmatism in the Tannuola subzone [54]. The growth of the back-arc ophiolites and basalts continues in the Agardag subzone (gabbro 546 ± 18 Ma [63]) but is also reported from the late Ediacaran Anakhem complex in the Ulugo back-arc subzone [98,99]. Sedimentary deposits began to develop largely across the suprasubduction “basement” in the forearc and back-arc regions.

Ediacaran to early Cambrian sediments of the forearc basin contain single interlayers of the late Chingin basalts. For the Duushkunnug hypabyssal gabbro massif located near the Saryg-Tash site (Figure 1), an age of 537.5 ± 4.9 Ma (Ar–Ar dating on amphibole) was determined, which shows an E-MORB-like composition with weakly pronounced island arc characteristics [100]. In addition, bodies of the Izinziul’ microgabbro-diorite-plagiogranite subvolcanic complex, including E-MORB-like diabase-microgabbros, dated at 538 ± 4 Ma (unpublished data, SHRIMP-II analysis of zircons from plagiogranite on the right bank of the Izinziul’ River), are associated with the Chingin basalts (see Table S1). The age of the Duushkunnug gabbro and our unpublished preliminary data imply a magmatic forearc impulse at about 538 Ma, which is likely linked to the emplacements of the late Chingin basalts. The source(s) of these later E-MORB-like forearc magmatites (compare mantle wedge in Figure 11e) remains uncertain. If their genesis was explained using the “accretionary model,” the gabbro of the Duushkunnug massif, the Izinziul’ complex, and the late Chingin basalts were magmatic bodies that intruded the accretionary prism during subduction (accretion and collision of the oceanic plateau and the Tannuola-Khamsara island arc began at the Ediacaran – Cambrian boundary, although subduction continued until the middle of the early Cambrian [54]). However, the stratigraphic intact arrangement of the late Chingin basalts and the predominant localization of subvolcanic bodies of the Izinziul’ complex on the boundary of the lower and upper Chingin subformations make it unlikely that those magmatics intruded the accretionary prism itself as, e.g., unrelated irregular dikes.

Data by Borisova et al. infer that the chemical evolution of oceanic basaltic magmas depends on (1) the depth of their interaction with the overlying oceanic lithospheric mantle (serpentinized by seawater-derived fluids) and (2) the rate of the basaltic melt transport from their upper mantle source, i.e., the time the oceanic melts interacted with the serpentinized lithospheric mantle [101]. These data are not completely consistent with our proposed model of forearc basalt genesis in the Sayan-Tuvan forearc zone, but they emphasize the importance of oceanic crust thickness for composition of mantle-derived basaltic melts.

5.3.5 Possible causes of mantle melting and the influence of oceanic crust thickness on basalt formation

Recent observations of the Hawaiian plume systems [75] indicate the degree of partial melting and trace element

contents may be strongly depended on the thickness of the oceanic crust (but see also Section 5.3.4). In the case of the Sayan-Tuvan forearc zone, this mechanism may have influenced the formation of the enriched early Aldynbulak basalts over thicker crust followed by the depleted Uttug-Khaia basalts and the Chingin basalts (and boninites) and also Uttug-Khaia dikes which formed over the relative thinner parts of the crust caused by spreading. This process has also been suggested to explain the co-occurrence of geochemically different basalts in a similar geodynamic setting in the Paleo-Asian Ocean, the Gorny Altai accretionary prism (Kuznetsk-Altai, Figure 1a) [29]. General decompression melting most likely took place in response to the subduction initiation, slab rollback, and overall thinning of the crust. We argue that the mantle melting was not caused by a mantle plume but by another process of supraregional tectonic nature and scale, which led to the initiation of subduction – followed by decompression melting of the mantle. The Aldynbulak basalts differ from the subsequent generations of Uttug-Khaia and Chingin basalts by lower degrees of partial melting of the mantle and larger proportions of enriched sources. Possibly, the changing basalt geochemistry was caused by a thinning of the oceanic crust over the area of mantle magma generation as a result of suprasubduction spreading.

5.4 Implications for the ASFB

The results and interpretation of the basalts in this study may also create implications for similar geological settings in the ASFB. In the forearc zone of the Gorny Altai terrane, OIB-like basalts are present in the Manzherok Formation in the Katun zone (initial ε_{Nd} = +0.9 to +5.2) and enriched to transitional basalts (initial ε_{Nd} for transitional basalts: +7.8 to +8.1) in the Kurai zone [21,29]. Some samples of the enriched and transitional basalts show a negative Nb anomaly and N-MORB-like composition. Basalts depleted in Nb are present in both, the Katun and Kurai zones, suggesting an association with subduction zones [61]. All these basalts are usually interpreted as part of seamounts that were incorporated into accretionary prisms [20,21,29]. There are substantial (geochemical) facies analogies between the enriched and OIB-like Kurai and Aldynbulak basalts, the enriched and transitional Kurai zone and Chingin basalts, as well as N-MORB-like basalts of the Katun and Kurai zones and Uttug-Khaia basalts. Paleospreading complexes associated with the Kurai basalts even comprise boninite-bearing units [16].

In the collisional zone of the Dzhida island arc system, basite-hyperbasite ophiolite complexes, boninite-basalt units, oceanic islands, oceanic plateaus, and oceanic crust of the MOR-type have been identified. Island arc systems were superimposed on all these structures [28,30]. Trace element contents of most Dzhida ocean plateau and ocean crust basalts show a negative Nb anomaly signaling a subduction-related origin – comparable to the patterns seen in the basalts in the Gorny Altai and the Sayan-Tuvan forearc zone.

In the northern part of the adjacent Lake Zone island arc system (Figure 1a), which extends south from Tuva to western Mongolia, island arc basalts, basalts of E- and N-MORB-like composition were recognized. The geochemical properties of these basalts (strong depletion in incompatible elements (Th-La), no or minor Nb–Ta anomaly, and negligible or positive Ti anomaly) indicate that the origin of these rocks is associated with geodynamic environments comparable to mantle plume related oceanic islands or lava plateaus [102]. The composition of the Lake Zone basalts, however, also seem to reflect processes of melt mixing, with the end members being suprasubductional, N-MORB, and OIB or E-MORB types. The rocks of all three types were generated simultaneously in the same marginal ocean basin in the Lake Zone [103]. Given the close spatial context and similar timing of formation, subduction initiation mechanisms could also explain the origin of these rocks in the Lake Zone.

In a review of ophiolitic outcrops throughout the Central Asian Orogenic Belt, Yang et al. [32] re-assigned a significant number of ophiolites to suprasubduction or suprasubduction/plume-type ophiolites, which only further shows the need for detailed studies of subduction initiation processes throughout the ASFB and the possible implications this may have for paleogeographic and geodynamic reconstructions.

6 Conclusion

This article presents a new look at the geodynamic position of the basalts of the Aldynbulak, Uttug-Khaia, and Chingin strata, which were often considered parts of unrelated oceanic structures accreted into the forearc zone of the Tannuola-Khamsara island arc.

The igneous forearc complexes of the Tannuola-Khamsara island arc are represented by metamorphic units in the accretionary prism of the Dzhebash Group, which include (intraplate) oceanic plateau basalts, as well as subduction-related rocks, that formed during protoarc–forearc settings during the early stages of the subduction. The rock

suites that are considered part of the protoarc–forearc stage are the frontal paleospreading complexes of the Kurtushiba ophiolites and the closely related volcano-sedimentary and basalt-bearing Chingin Formation. The basalt-sedimentary Aldynbulak and Uttug-Khaia formations and paleospreading complexes of the Khemchik ophiolites were generated at some distance to the trench. These coherences are assumed from today's tectonic and stratigraphic positions of those units. The evaluation of the geologic history of the enriched forearc basalts of the Aldynbulak, Uttug-Khaia, and Chingin formations shows that their magmas evolved from an OIB-like to MORB-like composition. This geochemical trend could be the result of different degrees of decompression partial melting depending on the thickness of the crust above it – the thinner the crust, the higher the degree of partial melting and *vice versa*.

We propose that the first tectonomagmatic event was decompression melting of the predominantly deep mantle at low degrees of partial melting. The cause for the subduction initiation which led to the decompression melting during the middle Ediacaran remains speculative. During the initial stages, the enriched Aldynbulak basalts of OIB + E-MORB-like composition were formed (located above the relative thickest parts of oceanic crust). Following the subduction initiation, a slab rollback led to stretching and spreading in the upper plate and the formation of ophiolite complexes under the influence of decompression and fluid-flux melting of the depleted mantle (the thinnest crust). When the slab rollback slowed down and the transition to normal subduction began, Uttug-Khaia and Chingin basalts of N– and E + T-MORB-like composition formed due to varying mixing ratios of enriched and depleted melts. Boninite lavas were emplaced onto the newly formed forearc crust (average crust thickness). The Chingin and Uttug-Khaia formation basalts indicate a forearc magmatic affinity according to a Tb*3–Th–Ta*2 diagram (Figure 9c) (after [74]), which coincides with the results of Mongush [59], that the Khemchik and Kurtushiba ophiolites are forearc plateau-like rocks.

We conclude that these basalts were formed in the protoarc–forearc zone during the initial stages of subduction. Arguments that speak against a simple suture zone-like accretion of the Sayan-Tuvan forearc zone terranes and for a subduction initiation setting origin are summarized as follows:

1) Conformable contact of the Chingin Formation and the Kurtushiba ophiolites, the presence of boninites among both, the Chingin basalts and as dikes within the Kurtushiba ophiolite (Sections 2.2.1, 2.2.2, and 2.4.1).
2) Geochemical and geochronological similarity of Kurtushiba and Khemchik (~578 Ma) [37] ophiolites with the early island-arc igneous rocks of the Ondum subzone (beginning from ~572 Ma) [39] (Section 2.4.3).
3) Forearc magmatic affinity of the Khemchik and Kurtushiba ophiolites [59], as well as the Chingin and Uttug-Khaia basalts (Section 4.2.1).
4) Earliest Cambrian (538 Ma) [100] E-MORB-like magmatic bodies within the Chingin subformations (Section 5.3.4), which indicate a late stage of forearc magmatism.
5) Early Cambrian forearc- and middle Cambrian molasse basin-style sedimentation form connecting overlap assemblages throughout the forearc basin (Section 5.1).
6) If the Aldynbulak and Uttug-Khaia formations and the Khemchik ophiolites, Chingin Formation, and the Kurtushiba ophiolites were accretioned formations, then the protoarc–forearc zone between the Dzhebash accretion prism and the Tannuola-Khamsara island arc would not exist in the way it does today, i.e., the entire space in front of the island arc would consist entirely of tectonically assembled units, which is not plausible (Figure 1b–d, Section 4.2.2).

Our results further imply that similar basalt and ophiolite suites found throughout the ASFB need to be investigated if these always truly represent accreted hotspot-related seamounts or oceanic plateau structures, as suprasubduction ophiolites may be more widespread as previously acknowledged [32]. Future tectonostratigraphic, petrologic studies and precise age dating of the proposed forearc basalts will contribute to a better understanding of the formation patterns of the Ediacaran–early Paleozoic structures of the ASFB and Central Asian Orogenic Belt.

Acknowledgements: We wish to thank our colleagues V. A. Popov and R. V. Kuzhuget for joint field work, E. K. Druzhkova for assistance in petrographic analysis, D. P. Gorbunov and L. K. Gorshkova for the preparation of samples and thin sections as well as E. V. Smirnova, A. L. Finkel'shtein, P.A. Serov, S. V. Palessky, and Ya. V. Bychkova for analytical research. This study was funded by a research grant from the Russian Foundation for Basic Research (17-05-00190) and basic research projects of the Tuvinian Institute for the Exploration of Natural Resources of the Russian Academy of Sciences Siberian Branch (No. 121031500140-2). P. Olschewski was not funded by any specific grants for this project, but we thank the Memorial University Libraries' "Open Access Author Fund" initiative for supporting this open access publication. We also highly appreciated the constructive input and suggestions by the two anonymous reviewers.

Author contributions: A.M. and P.O. contributed to this study in equal amounts. A.M. conducted and organized the field work in Russia and the analytical research in

the laboratory (for a list of collaboration partners the reader is referred to the acknowledgement section). A.M. also interpretated the data, wrote the initial draft, compiled a first reference list, and created the figures and tables. P.O. contributed to this work by translating, editing, and re-arranging the text, figures, tables, and references; helped with discussion of results, additional literature research, and agreeing to be corresponding author.

Conflict of interest: The authors declare no conflicts of interests of which they are aware of.

Data availability statement: Data is available upon request by contacting any of the authors.

References

[1] Pearce JA, Lippard SJ, Roberts S. Characteristics and tectonic significance of suprasubduction zone ophiolites. In: Kokelaar BP, Howells MF, editors. Marginal Basin Geology: Volcanic and Associated Sedimentary and Tectonic Processes in Modern and Ancient Marginal Basins. Geol Soc London Special Publication no. 16. Oxford, London, Edinburgh, Boston, Palo Alto, Melbourne: Blackwell Scientific Publications; 1984. p. 77–94.

[2] Casey JF, Dewey JF. Initiation of subduction zones along transform and accreting plate boundaries, triple junction evolution and spreading centres – Implications for ophiolitic geology and obduction. In: Gass GI, Lippard SJ, Shelton AW, editors. Ophiolites and Oceanic Lithosphere. Geol Soc London Special Publication no. 13. Oxford, London, Edinburgh, Boston, Palo Alto, Melbourne: Blackwell Scientific Publications; 1984. p. 269–90.

[3] Bloomer SH, Taylor B, MacLeod CJ, Stern RJ, Fryer P, Hawkins JW et al. Early arc volcanism and the ophiolite problem: A perspective from drilling in the western Pacific. In: Taylor B, Natland J, editors. Active Margins and Marginal Basins of the Western Pacific. Geophys Monogr Ser. Vol. 88. Washington D. C: American Geophysical Union; 1995. p. 67–96.

[4] Pearce JA, Robinson PT. The Troodos ophiolitic complex probably formed in a subduction initiation, slab edge setting. Gondwana Res. 2010;18:60–81.

[5] Wakabayashi J, Ghatak A, Basu AR. Suprasubduction-zone ophiolite generation, emplacement, and initiation of subduction: A perspective from geochemistry, metamorphism, geochronology, and regional geology. Geol Soc Am Bull. 2010;122(9–10):1548–68.

[6] Stern RJ, Reagan M, Ishizuka O, Ohara Y, Whattam S. To understand subduction initiation, study forearc crust: To understand forearc crust, study ophiolites. Lithosphere – US. 2012;4(6):469–83.

[7] Maffione M, Thieulot C, van Hinsbergen DJJ, Morris A, Plumper O, Spakman W. Dynamics of intraoceanic subduction initiation: 1. Oceanic detachment fault inversion and the formation of supra-subduction zone ophiolites. Geochem Geophys Geosyst. 2015;16(6):1753–70.

[8] Reagan MK, Pearce JA, Petronotis K, Almeev RR, Avery AJ, Carvallo C, et al. Subduction initiation and ophiolite crust: New insights from IODP drilling. Int Geol Rev. 2017;59(11):1439–50.

[9] Bebien J, Dimo-Lahitte A, Vergély P, Insergueix-Filippi D, Dupeyrat L. Albanian ophiolites. I – Magmatic and metamorphic processes associated with the initiation of a subduction. Ofioliti. 2000;25(1):39–45.

[10] Dilek Y, Furnes H. Structure and geochemistry of Tethyan ophiolites and their petrogenesis in subduction rollback systems. Lithos. 2009;113:1–20.

[11] Dilek Y, Furnes H. Ophiolite genesis and global tectonics: Geochemical and tectonic fingerprinting of ancient oceanic lithosphere. Geol Soc Am Bull. 2011;123(3/4):387–411.

[12] Whattam SA, Stern RJ. The 'subduction initiation rule': a key for linking ophiolites, intra-oceanic forearcs, and subduction initiation. Contrib Miner Petr. 2011;162:1031–45.

[13] Shervais JW, Reagan M, Haugen E, Almeev RR, Pearce JA, Prytulak J, et al. Magmatic response to subduction initiation: Part 1. Fore-arc basalts of the Izu-Bonin arc from IODP Expedition 352. Geochem Geophys Geosyst. 2019;20:314–38.

[14] Berzin NA, Kungurtsev LV. Geodynamic interpretation of Altai-Sayan geological complexes. Geol Geofiz. 1996;37(1):56–73 (in Russian with English summary).

[15] Dobretsov NL, Buslov MM, Uchio Y. Fragments of oceanic islands in accretion-collision areas of Gomy Altai and Salair, southern Siberia, Russia: early stages of continental crustal growth of the Siberian continent in Vendian - Early Cambrian time. J Asian Earth Sci. 2004;23:673–90.

[16] Dobretsov NL, Simonov VA, Buslov MM, Kotlyarov AV. Magmatism and geodynamics of the Paleoasian ocean at the Vendian-Cambrian stage of its evolution. Russ Geol Geophys. 2005;46(9):933–51.

[17] Buslov MM, Watanabe T, Saphonova IYu, Iwata K, Travin A, Akiyama MA. Vendian-Cambrian Island Arc system of the Siberian Continent in Gorny Altai (Russia, Central Asia). Gondwana Res. 2002;5(4):781–800.

[18] Yarmolyuk VV, Kovalenko VI, Kovach VP, Kozakov IK, Kotov AB, Sal'nikova EB. Geodynamics of caledonides in the Central Asian Foldbelt. Dokl Earth Sci. 2003;389(3):311–6.

[19] Yarmolyuk VV, Kovalenko VI, Kovach VP, Rytsk E Yu, Kozakov IK, Kotov AB, et al. Early stages of the paleoasian ocean formation: results of geochronological, isotopic, and geochemical investigations of late Riphean and Vendian–Cambrian complexes in the Central Asian Foldbelt. Dokl Earth Sci. 2006;411(8):1184–9.

[20] Safonova IYu, Simonov VA, Buslov MM, Ota T, Maruyama Sh. Neoproterozoic basalts of the Paleo-Asian Ocean (Kurai accretionary zone, Gorny Altai, Russia): geochemistry, petrogenesis, and geodynamics. Russ Geol Geophys. 2008;49(4):254–71.

[21] Safonova IYu, Buslov MM, Simonov VA, Izokh AE, Komiya T, Kurganskaya EV, et al. Geochemistry, petrogenesis and geodynamic origin of basalts from the Katun' accretionary complex of Gorny Altai (southwestern Siberia). Russ Geol Geophys. 2011;52(4):421–42.

[22] Volkova NI, Stupakov SI, Babin GA, Rudnev SN, Mongush AA. Mobility of trace elements during subduction metamorphism as exemplified by the blueschists of the Kurtushibinsky range, Western Sayan. Geochem Int. 2009;47(4):380–92.

[23] Kheraskova TN, Didenko AN, Bush VA. The Vendian-Early Paleozoic history of the continental margin of eastern

paleogondwana, Paleoasian ocean, and Central Asian foldbelt. Russ J Earth Sci. 2003;5(3):165–84.
[24] Wilhem C, Windley BF, Stampfli GM. The altaids of Central Asia: A tectonic and evolutionary innovative review. Earth Sci Rev. 2012;113(3–4):303–41.
[25] Safonova IYu, Santosh M. Accretionary complexes in the Asia-Pacific region: Tracing archives of Ocean Plate Stratigraphy and tracking mantle plumes. Gondwana Res. 2014;25:126–58.
[26] Şengör AC, Sunal G, Natal'in BA, Van der Voo R. The Altaids: A review of twenty-five years of knowledge accumulation. Earth Sci Rev. 2022;228:104013. doi: 10.1016/j.earscirev.2022.104013
[27] Shervais JW, Choi SH. Subduction initiation along transform faults: The proto-Franciscan subduction zone. Lithosphere-US. 2012;4(6):484–96.
[28] Gordienko IV, Filimonov AV, Minina OR, Klimuk VS, Elbaev AL, Gornova MA, et al. Dzhida island arc system in the Paleoasian ocean: Structure and main stages of Vendian–Paleozoic geodynamic evolution. Russ Geol Geophys. 2007;48(1):91–106.
[29] Safonova IYu. Geochemical evolution of intraplate magmatism in the Paleo-Asian Ocean from the late Neoproterozoic to the early Cambrian. Petrology. 2008;16(5):492–511.
[30] Simonov VA, Stupakov SI, Kotlyarov AV, Kovyazin SV, Gordienko IV, Medvedev AY. Conditions of basalt formation in the Dzhida zone of the Paleoasian Ocean. Russ Geol Geophys. 2014;55(8):929–40.
[31] Furnes H, Safonova IYu. Ophiolites of the Central Asian orogenic belt: geochemical and petrological characterization and tectonic setting. Geosci Front. 2019;10(4):1255–84. doi: 10.1016/j.gsf.2018.12.007
[32] Yang G, Li Y, Tong L, Wang Z, Si G, Lindagato P, et al. Natural observations of subduction initiation: Implications for the geodynamic evolution of the Paleo-Asian Ocean. Geosyst Geoenviron. 2022;1(1):100009. doi: 10.1016/j.geogeo.2021.10.004
[33] Pearce JA, Reagan MK. Identification, classification, and interpretation of boninites from Anthropocene to Eoarchean using Si-Mg-Ti systematics. Geosphere. 2019;15(4):1008–37.
[34] Slovenec D, Šegvić B. Boninite volcanic rocks from the mélange of NW Dinaric-Vardar ophiolite zone (Mt. Medvednica, Croatia) - record of Middle to Late Jurassic arc-forearc system in the Tethyan subduction factory. Min Pet. 2019;113(1):17–37.
[35] Aleksandrovsky YuS, Alekseenko VD, Belyaev GM, Bluman BA, Bulychev AV, Dolzhkovoi BM et al. State geological map of the Russian Federation. Scale 1:1.000.000. Series of the Altai-Sayan. Sheet M-46 - Kyzyl. Explanatory note. 3rd edn. St. Petersburg: VSEGEI Cartographic Service; 2008 (in Russian).
[36] Bezzubtsev VV, Makhlaev ML, Kirichenko VT, Perfilova OYu, Yurkevich LG, Markovich LA et al. State geological map of the Russian Federation. Scale 1:1.000.000. Series of the Altai-Sayan. Sheet N-46-Abakan. Explanatory note. 3rd edn. St. Petersburg: VSEGEI Cartographic Service; 2008 (in Russian).
[37] Mongush AA, Lebedev VI, Travin AV, Yarmolyuk VV. Ophiolites of western Tyva as fragments of a late Vendian Island arc of the Paleoasian Ocean. Dokl Earth Sci. 2011;438(2):866–72.
[38] Rudnev SN, Kiseleva VY, Serov PA. Vendian - early Paleozoic granitoid magmatism in Eastern Tuva. Russ Geol Geophys. 2015;56(9):1232–55.
[39] Rudnev SN, Mal'kovets VG, Belousova EA, Turkina OM, Semenova DV. Lu–Hf Isotope composition of zircon and magma sources of the Vendian–early paleozoic granitoids in Tuva (by the Example of the Kaa-Khem and East Tannu-Ola Batholiths). Russ Geol Geophys. 2020;61(10):1088–1108.
[40] Astashkin VA, Belyaeva GV, Esakova NV, Osadchaya DV, Pakhomov NN, Pegel TV, et al. The Cambrian system of the foldbelts of Russia and Mongolia: correlation chart and explanatory notes. International Union of Geological Sciences. International Commission of Stratigraphy; 1995, No. 32
[41] Dobretsov NL, Buslov MM. Late Cambrian - Ordovician tectonics and geodynamics of Central Asia. Russ Geol Geophys. 2007;48(1):71–82.
[42] Berzin NA. Geodynamic situation for the formation of Cambrian olistostromes in Khemchikski-Sistigkhemskaya zone of Tuva. Geol Geofiz. 1987;28(1):3–11 (in Russian with English summary).
[43] Berzin NA. Preliminary terrane and overlap assemblage map of Altay - Sayan region, southern Siberia, Russia. In: Nokleberg WJ, Naumova VV, Mikhail IK, Bouaeva TV, editors. Preliminary publications book 1 from project on mineral resources, metallogenesis, and tectonics of northeast Asia. U.S. Department of the Interior, USGS; 1999. Open-File Report 99-165. doi: 10.3133/ofr99165.
[44] Dobretsov NL, Ponomareva LG. Ophiolites Glaucophane schists in West Sayan and Kurtushibinsk belt. In: Sobolev VS, Dobretsov NL, editors. Petrology and metamorphism of ancient ophiolites (as example of polar Ural and West Sayan). Novosibirsk: Nauka; 1977. p. 128–56. (in Russian with English index)
[45] Popov VA, Mitus AI, Nechaeva SP. State geological map of the Russian Federation scale 1:200.000. Series of West-Sayan. Sheet N-46-XXIX (Upper Amyl). Explanatory note. 2nd edn. St. Petersburg: VSEGEI Cartographic Service; 2003 (in Russian).
[46] Lyashenko OV. Comparative tectonics of the Kurtushiba and East Sayan ophiolite belts (Altai-Sayan folded area). Russia: University of Moscow; 1984. PhD thesis (in Russian).
[47] Mongush AA, Kadyrool ChO, Druzhkova EK, Oidup ChK, Timoshenko EN. Basalts with spinifex-pyroxene structure in the Chingin Formation at the Koiard site (Kurtushiba ridge of the Western Sayan). Tectonics and geodynamics of the Earth's crust and mantle: fundamental problems – 2023. Moscow: Materials of the LIV (54) Tectonic Meeting; 2023 (in Russian).
[48] Dyatlova IN. New data in the geological structure and stratigraphy of the Kurtushibinsky structural-formation zone of the Western Sayan within the Verkhneamylsky gold cluster. Nat Res Env Soc. 2022;4(16):21–36. (in Russian with English abstract) doi: 10.24412/2658-4441-2022-4-21-36
[49] Mongush AA, Terleev AA, Tokarev DA, Druzhkova YK. Granitoids and limestones from conglomerates of forearc of Tannuola–Khamsara island arc system (Tuva): geochemistry, paleontology, correlation. Tomsk State Univ J. 2013;372:184–92 (in Russian with English abstract).
[50] Brodnikova EA, Vetrov EV, Letnikova EF, Ivanov AV, Rudnev SN. Early Ediacaran and middle Ediacaran granitoids in the provenances of early Cambrian coarse-grained rocks of the Bayan-kol Formation of the Systyg-Khem depression (Tuva). Russ Geol Geophys. 2022;63(6):649–63.
[51] Shcherbakov SA. Ophiolites of Western Tuva and their structural position. In: Pushcharovskij YuM, Mossakovsky AA, Burtman VS, Schuplezova MN, Zaborovskaya NB, Samygin SG, editors. Geotektonika. Vol. 4. Moscow: Academy of Sciences of the USSR; 1991. p. 88–101 (in Russian with English index).
[52] Peng SC, Babcock LE, Cooper RA. The Cambrian Period. In: Gradstein FM, Ogg JG, Schmitz MD, Ogg GM, editors. The geologic

time scale. Vol. II. Amsterdam, Oxford, Cambridge: Elsevier; 2020. p. 565–629.
[53] Nokleberg WJ, Badarch G, Berzin NA, Diggles MF, Hwang DH, Khanchuk AI, et al. Digital files for Northeast Asia geodynamics, mineral deposit location, and metallogenic belt maps, stratigraphic columns, descriptions of map units, and descriptions of metallogenic belts. Open-File Rep 2004-1252. US Department of the Interior, USGS; 2004. doi: 10.3133/ofr99165.
[54] Mongush AA, Lebedev VI, Kovach VP, Sal'nikova EB, Druzhkova EK, Yakovleva SZ, et al. The tectonomagmatic evolution of structure-lithologic complexes in the Tannu-Ola zone, Tuva, in the Late Vendian–Early Cambrian (from geochemical, Nd isotope, and geochronological data). Russ Geol Geophys. 2011;52(5):503–16.
[55] Lesnov FP, Kuzhuget KS, Mongush AA. Geology, petrology and ore-bearing of mafic-ultramafic massifs in the Republic of Tuva. Geo, Novosibirsk; 2019 (in Russian).
[56] Simonov VA, Dobretsov NL, Buslov MM. Boninite series in the structures of the Paleoasian Ocean. Geol Geofiz. 1994;35(7–8):182–99 (in Russian with English summary).
[57] Kurenkov SA, Didenko AN, Simonov VA. Geodynamics of paleospreading. Moscow: GEOS; 2002 (in Russian with English summary).
[58] Chernyshov AI, Vorobyeva AV, Yurichev AN. Petrology of mafic-ultramafic Kizir-Burluksky massif (Northeast of Western Sayan). Bull Tomsk Polytechnic University. Geo Assets Eng. 2020;331(8):199–20. doi: 10.18799/24131830/2020/8/2781 (in Russian with English summary).
[59] Mongush AA. Geological position, geochemical and Sm-Nd-isotopic composition of ophiolites of the Sayan-Tuva Forearc zone. Bull Irkutsk State Univ. 2019;30:56–75. doi: 10.26516/2073-3402.2019.30.56 (in Russian with English summary).
[60] Pearce JA. Trace element characteristics of lavas from destructive plate boundaries. In: Thorpe ES, (editor). Andesites: Orogenic andesites and related rocks. New York: Wiley; 1982. p. 526–47.
[61] Baier J, Audétat A, Keppler H. The origin of the negative niobium tantalum anomaly in subduction zone magmas. Earth Planet Sci Lett. 2008;267(1–2):290–300.
[62] Pearce JA, van der Laan SR, Arculus RJ, Murton BJ, Ishii T, Peate DW et al. 38. Boninite and harzburgite from ODP Leg 125 (Bonin-Mariana forearc): A case study of magma genesis during the initial stages of subduction. Proceedings Of The Ocean Drilling Program, Scientific Results. Vol. 125. 1992. p. 623–59.
[63] Pfänder JA, Kröner A. Tectono-magmatic evolution, age and emplacement of the Agardagh Tes-Chem ophiolite in Tuva, Central Asia: Crustal growth by island arc accretion. In: Kusky TM, editor. Precambrian Ophiolites and Related Rocks. Developments in Precambrian Geology. Vol. 13. Amsterdam: Elsevier; 2004. p. 207–21.
[64] Ivanov AV, Letnikova EF, Shkolnik SI, Maslov AV, Vetrova NI. Early Cambrian deposits of the continental margin (South of Tuva, Teregtig Formation): results of U–Pb dating of detrital zircons and Sr-chemostratigraphy. Dokl Earth Sci. 2023;512:915–22.
[65] Pfänder JA, Jochum KP, Kozakov I, Kröner A, Todt W. Coupled evolution of back-arc and island arc-like mafic crust in the late-Neoproterozoic Agardagh Tes-Chem ophiolite, Central Asia: evidence from trace element and Sr-Nd-Pb isotope data. Contrib Miner Petr. 2002;143:154–74.
[66] Pfänder JA, Jochum KP, Galer SJG, Hellebrand EWG, Jung S, Kröner A. Geochemistry of ultramafic and mafic rocks from the northern Central Asian Orogenic Belt (Tuva, Central Asia) - constraints on lower and middle arc crust formation linked to late Proterozoic intra oceanic subduction. Precambrian Res. 2021;356:1–22. doi: 10.1016/j.precamres.2020.106061.
[67] Mongush AA, Kuzhuget RV, Druzhkova EK. Different types of basalts of the Tes-Khem site of the Agardag back-arc subzone (Tuva): Material composition and possible geodynamic position. Geosph Res. 2023;2:6–17 (in Russian with English summary).
[68] Bukharov NS. On the Vendian - early Cambrian deposits in the Tapsa, Cherbin and Ondum River valleys (central Tuva). In: Podkamenny AA, editor. Materials on the geology of the ASSR Tuva. Vol. 5. Kyzyl: Tuva Press; 1981. p. 58–63 (in Russian).
[69] Le Bas MJ, Le Maitre RW, Streckeisen A, Zanettin B. A Chemical classification of volcanic rocks based on the total alkali-silica diagram. J Pet. 1986;27:745–50.
[70] Condie KC. High field strength element ratios in Archean basalts: a window to evolving sources of mantle plumes? Lithos. 2005;79:491–504.
[71] Meschede M. A method of discriminating between different types of mid-ocean ridge basalts and continental tholeiites with the Nb-Zr-Y diagram. Chem Geol. 1986;56(3–4):207–18.
[72] Sun SS. McDonough WF. Chemical and isotopic systematics of oceanic basalts: implications for mantle composition and processes. In: Saunders AD, Norry MJ, editors. Magmatism in the Ocean Basins. Geol Soc London Special Publication. No. 42. Oxford, London, Edinburgh, Boston, Palo Alto, Melbourne: Blackwell Scientific Publications; 1989. p. 313–46.
[73] Klein EM. Geochemistry of the igneous ocean crust. In: Rudnick RL, editor. Treatise on Geochemistry. Vol. 3. Amsterdam: Elsevier; 2003. p. 433–63.
[74] Cabanis B, Thiéblemont D. Discrimination of continental tholeiites and back-arc basin basalts using the Th-3 × Tb × Ta*2 diagram. Bull Soc Geol Fr. 1988;8(6):927–35 (in French with English summary).
[75] Regelous M, Hofmann AW, Abouchami W, Galer SJG. Geochemistry of lavas from the Emperor Seamounts, and the geochemical evolution of Hawaiian magmatism from 85 to 42 Ma. J Pet. 2003;44(1):113–40.
[76] Sun SS, Nesbitt RW, Sharaskin AY. Geochemical characteristics of mid-ocean ridge basalts. Earth Planet Sc Lett. 1979;44(1):119–38.
[77] Wilson M. Igneous petrogenesis. A global tectonic approach. 1st edn. 2007 reprint. Dordrecht: Springer; 1989.
[78] Xia L, Li X. Basalt geochemistry as a diagnostic indicator of tectonic setting. Gondwana Res. 2019;65:43–67.
[79] Hofmann AW. Mantle geochemistry: the message from oceanic volcanism. Nature. 1997;385:219–29.
[80] DePaolo JD. Neodymium isotope geochemistry. An introduction. Minerals and Rocks. Vol. 20. Berlin, Heidelberg, New York, London, Paris, Tokyo: Springer-Verlag; 1988.
[81] Kovalenko VI, Yarmolyuk VV, Kovach VP, Kotov AB, Sal'nikova EB. Magmatism and geodynamics of early Caledonian structures of the Central Asian fold belt (isotope and geological data). Russ Geol Geophys. 2003;44(12):1235–48.
[82] Kuzhuget KS, Oidup ChK. Some features of the relationship between the basic and ultrabasic rocks of the Kyzyr-Burlyuk massif (Western Sayan). In: Zolotuhin VV, editor. Hyperbasite associations of fold belt regions. Vol. 4, Novosibirsk: Institute of Geology and Geophysics; 1987. p. 96–106 (in Russian).
[83] Sklyarov EV, Kovach VP, Kotov AB, Kuzmichev AB, Lavrenchuk AV, Perelyaev VI, et al. Boninites and ophiolites: Problems of their relations and petrogenesis of boninites. Russ Geol Geophys. 2014;57(1):127–40.

[84] Shervais JW, Choi SH, Sharp WD, Ross J, Zoglman-Schuman M, Mukasa SB. Serpentinite matrix mélange: Implications of mixed provenance for mélange formation. In: Wakabayashi J, Dilek Y, editors. Mélanges: Processes of formation and societal significance. Geol S AM S, 2011;480:1–31.
[85] Festa A, Ogata K, Pini GA, Dilek Y, Alonso JL. Origin and significance of olistostromes in the evolution of orogenic belts: A global synthesis. Gondwana Res. 2016;39:180–203.
[86] Festa A, Barbero E, Remitti F, Ogata K, Pini GA. Mélanges and chaotic rock units: Implications for exhumed subduction complexes and orogenic belts. Geosyst Geoenviron. 2022;1(2):1–23. doi: 10.1016/j.geogeo.2022.100030
[87] Ogata K, Festa A, Pini GA, Pogačnik Ž, Lucente CC. Substrate deformation and incorporation in sedimentary mélanges (olistostromes): Examples from the northern Apennines (Italy) and northwestern Dinarides (Slovenia). Gondwana Res. 2019;74:101–25.
[88] Wakabayashi J. Sedimentary compared to tectonically-deformed serpentinites and tectonic serpentinite mélanges at outcrop to petrographic scales: Unambiguous and disputed examples from California. Gondwana Res. 2019;74:51–67.
[89] Osadchaya DV, Kotel'nikov DS. Archaeocyathids from the Atdabanian (Lower Cambrian) of the Altay Sayan Foldbelt, Russia. Geodiversitas. 1998;20(1):5–18.
[90] Korovnikov IV, Novozhilova NV, Tokarev DA. Distribution of Atdabanian (Early Cambrian) trilobites, archaeocyaths, and small shelly fossils in the Altai–Sayan folded area. Paleontol J. 2018;52:1481–93.
[91] Stern RJ, Bloomer SH. Subduction zone infancy: examples from the Eocene Izu-Bonin-Mariana and Jurassic California arcs. Geol Soc Am Bull. 1992;104:1621–36.
[92] Reagan MK, Ishizuka O, Stern RJ, Kelley KA, Ohara Y, Blichert-Toft J, et al. Fore-arc basalts and subduction initiation in the Izu-Bonin-Mariana system. Geochem Geophys Geosyst. 2010;11(3):Q03X12. doi: 10.1029/2009GC002871
[93] Ishizuka O, Kimura JI, Li YB, Stern RJ, Reagan MK, Taylor RN, et al. Early stages in the evolution of Izu–Bonin arc volcanism: New age, chemical, and isotopic constraints. Earth Planet Sc Lett. 2006;250(1–2):385–401.
[94] Yogodzinski GM, Bizimis M, Hickey-Vargas R, McCarthy A, Hocking BD, Savov IP, et al. Implications of Eocene-age Philippine Sea and forearc basalts for initiation and early history of the Izu-Bonin-Mariana arc. Geochim Cosmochim Ac. 2018;228:136–56.
[95] Xin GY, Chu Y, Su BX, Lin W, Cui MM, Liu X, et al. Subduction initiation in the Neo-Tethys and formation of the Bursa ophiolite in NW Turkey. Lithos. 2022;422–3:1–17. doi: 10.1016/j.lithos.2022.106746
[96] Metcalf RV, Shervais JW. Suprasubduction-zone ophiolites: Is there really an ophiolite conundrum? In: Wright JE, Shervais JW, editors. Ophiolites, arcs, and batholiths: A Tribute to Cliff Hopson. Geol S AM S. 2008;438:191–222.
[97] Ishizuka O, Tani K, Reagan MK, Kanayama K, Umino S, Harigane Y, et al. The timescales of subduction initiation and subsequent evolution of an oceanic island arc. Earth Planet Sc Lett. 2011;306(3–4):229–40.
[98] Simonov VA, Zaikov VV, Kotlyarov AV, Terenya EO. "Petrological-geochemical features and paleogeodynamics of Cambrian magmatic complexes of Eastern Tuva". Probl Geol Geogr Sib. 2003;3:189–91. Tomsk (in Russian with English index).
[99] Zaykov VV. Volcanism and sulfide mounds of the paleocean margins (By the example of the Ural's and Siberia's massive sulfide-bearing zones). Moscow: Nauka; 2006 (in Russian).
[100] Mongush AA, Kuzhuget RV. Suprasubduction forearc gabbro of the Duushkunnug massif (Tuva): Unusual geochemical composition and the problem of geodynamic interpretation. Geosph Res. 2017;3:41–9 (in Russian with English summary).
[101] Borisova AY, Zagrtdenov NR, Toplis MJ, Ceuleneer G, Safonov OG, et al. Hydrated peridotite–basaltic melt interaction part II: Fast assimilation of serpentinized mantle by basaltic magma. Front Earth Sci. 2020;8:84. doi: 10.3389/feart.2020.00084
[102] Kovach VP, Yarmolyuk VV, Kovalenko VI, Kozlovskyi AM, Kotov AB, Terent'Eva LB. Composition, sources, and mechanisms of formation of the continental crust of the Lake Zone of the Central Asian Caledonides. II. Geochemical and Nd isotope data. Petrology. 2011;19:399–425.
[103] Kovalenko DV, Lebedev VI, Mongush AA, Sat KN, Ageeva OA, Koval'chuk EV. Geodynamics and sources of preaccretionary magmatism in western Mongolia. Petrology. 2016;24:178–95.
[104] Rickwood PC. Boundary lines within petrologic diagrams which use oxides of major and minor elements. Lithos. 1989;22:247–63.